UNIVERSITY OF LEEDS

This is a repository copy of *Pyridinic-nitrogen on ordered mesoporous carbon: A versatile NAD(P)H mimic for borrowing-hydrogen reactions*.

White Rose Research Online URL for this paper:
https://eprints.whiterose.ac.uk/196207/

Version: Accepted Version

White Rose
university consortium
Universities of Leeds, Sheffield & York

eprints@whiterose.ac.uk
https://eprints.whiterose.ac.uk/

Pyridinic-nitrogen on ordered mesoporous carbon: A versatile NAD(P)H mimic for borrowing-hydrogen reactions[†]

Talla V.R. Mohan [a‡], Madhu Nallagangula [b‡], Krishnan Kala[b‡], Carlos E. Hernandez-Tamargo[a‡], Nora H. De Leeuw [c,d], Kayambu Namitharan [b*], Venugopal T. Bhat [b*], (the late) Manickam Sasidharan[b§], and Parasuraman Selvam[a,e,f *]

[a]*National Centre for Catalysis Research and Department of Chemistry, Indian Institute of Technology-Madras, Chennai 600 036, India*

[b]*SRM Research Institute and Department of Chemistry, SRM Institute of Science and Technology, Kattankulathur 603 203, India*

[c]*School of Chemistry, Cardiff University, Cardiff CF10 3AT, United Kingdom*

[d]*School of Chemistry, University of Leeds, Leeds LS2 9JT, United Kingdom*

[e]*School of Chemical Engineering and Analytical Science, The University of Manchester, Manchester M13 9PL, United Kingdom*

[f]*International Research Organization for Advanced Science and Technology, Kumamoto University, Kumamoto 800-8555, Japan*

[†] *Supporting information is available for this article.*

[‡] *These authors contributed equally to this work.*

[§] *This paper is dedicated to the memory of our dear co-author Professor M. Sasidharan who passed away prematurely due to Covid-19 while this paper was being submitted/peer-reviewed.*

———————————————
[*]Corresponding authors. E-mail addresses:
namithak@srmist.edu.in (Kayambu Namitharan); venu.iitkgp@gmail.com (Venugopal T. Bhat); selvam@iitm.ac.in (P. Selvam)

1   **ABSTRACT**

2

3   Metal-free carbonaceous materials are an emerging class of heterogeneous catalysts for sustainable

4   chemistry. However, designing such catalytic materials with unique properties for specific organic

5   transformations remains a challenge due to an inadequate understanding of their active sites. Herein,

6   we report our studies on the use of nitrogen-doped ordered mesoporous carbons as a biomimetic novel

7   heterogeneous catalyst for the borrowing-hydrogen or hydrogen-auto-transfer class of cascade

8   reactions. These redox neutral processes have gained prominence owing to their high atom economy

9   and sustainability. Our experimental investigations, supported by computer modelling, show that the

10   local nitrogen environment, i.e., the benzannulated pyridine substructures on the edges/defects of the

11   carbon matrices, play a critical role as catalytic hydrogen shuttles in borrowing-hydrogen reactions

12   mimicking the role of the NAD(P)+/NAD(P)H redox couple.

13
14
15

INTRODUCTION

An enduring challenge in catalysis research is the realization of an ideal catalyst in terms of activity, selectivity, and atom economy for sustainable chemical processes. Currently, the field is dominated by transition metals either in the form of organometallic complexes, metal clusters, or nanoparticles [1,2]. However, there are serious concerns over the continuous availability of many of these precious metals as well as their environmental effects which provides an impetus for the development of alternate catalyst systems. In this context, there has been a renewed interest in the potential of abundant carbon materials in chemical catalysis. Carbonaceous materials are not new to heterogeneous catalysis with many metal-based catalysts utilizing them as supports due to their high surface area and stability. Recently, carbocatalysis or the direct application of carbon materials as heterogeneous catalysts for important organic transformations has gained traction [3,4]. These attempts have tried to utilize different functionalities in the carbon matrix as active sites for catalyzing organic transformations, including oxidations and acid/base catalyzed reactions [5,6]. A recent addition to the list of reactions catalyzed by carbon-based systems is the sp^2 carbon-carbon cross-coupling, a reaction closely related to the Suzuki-Miyaura coupling which uses Pd as a catalyst [7]. The reaction, in this case, was found to depend on the nature of the oxygen functionality in the carbon matrix [8]. These carbon systems have also been used for direct Friedel-Crafts alkylation reactions [9].

Despite the above advances in carbocatalysis, determining the exact nature of the catalytically active substructures in a heteroatom-doped carbon matrix is a difficult task. An in-depth understanding of these active structures coupled with an ability to tune them for specific organic transformations is integral to the development of carbocatalysts with high activity and selectivity. A general methodology adopted toward this goal is synthesizing a series of well-characterized heteroatom-doped catalysts and comparing their catalytic activities. A complementary approach is post-functionalization where the local substructure thought to be responsible for the activity is selectively introduced into the catalytically inactive carbon material through appropriate treatment. The appearance of activity, in this case, would be conclusive evidence of the nature of the active site embedded in the carbon matrix.

Nitrogen-doped/N-doped carbons have been in vogue for numerous applications, including electrocatalysis for the oxygen reduction reaction[10]. Recently, the N-alkylation of amines using a catalyst was reported, although the active sites on the carbon matrix responsible

for the transformation remained elusive[8]. These reactions follow a borrowing hydrogen (BH) or hydrogen auto-transfer (HAT) pathway and are important for the synthesis of a range of fine chemicals and pharmaceutical intermediates starting from cheap and readily available alcohols. These reactions have been well established for C–C and C–N bond formation and involve a series of steps, including an initial alcohol dehydrogenation followed by condensation and finally a reduction to yield the desired product. BH catalysis has so far relied on transition metal complexes to catalyze both the dehydrogenation and the reduction steps. Initial reports in this field dealt with noble metal-based homogeneous catalysts, e.g., Ir, Ru, Rh, which act as hydrogen shuttles transferring hydrogen from the initial alcohol to the final unsaturated intermediate[11-19]. Recently, base metal catalysts, e.g., Mn, Fe, and Co, have been developed as homogeneous catalysts for these processes[20-26]. However, these catalysts mostly require synthetically challenging ligands and additives. Likewise, heterogeneous supported metal catalysts have also been examined for BH catalysis[27,28]. However, the majority of these supported catalysts suffer from high catalyst leaching and poor reactivity associated with their harsh reaction conditions.

Inspired by the utility of N-doped carbons in these various C–C and C–N bond-forming processes, we focused on identifying and characterizing the active sites responsible for these reactions. The nitrogen species in these N-doped carbons are distributed in different local environments, e.g., graphitic (*grap*−N), pyridinic (*pyri*−N), and pyrrolic (*pyro*−N) nitrogen[29,30]. Among these, the *pyri*−N occurs as benzannulated pyridines distributed at the edges/defects of the N-doped carbon matrix [29], Figure 1-a, which is quite different from the nitrogen originating from the *g*-C_3N_4 structure[31], Figure 1-b. Recently, benzannulated pyridines such as phenanthridine and acridine have been utilized as NAD(P)H mimics in imine hydrogenation[32,33]. On this basis, we envisage that the benzannulated pyridines subunits at the edge/defect positions of N-doped carbon could mimic NAD(P)H and function as hydrogen shuttles in the BH cascade. In this regard, we have recently reported the successful synthesis of highly ordered 2D-hexagonal N-doped mesoporous carbons and their application in both chemical catalysis[34,35], electrocatalysis[36,37], and hydrogen storage[38-40], and carbon dioxide capture[41,42]. In this investigation, we present a detailed synthetic strategy and in-depth characterization of several such novel materials, and their applications in borrowing-hydrogen reactions, viz., N-alkylation of amines and ketones with primary alcohols, as well as C-alkylation of aromatic ketones and synthesis of quinolines by dehydrogenative condensation reactions between amino alcohols and ketones. In addition, the first examples of N-doped

carbon-catalyzed synthesis of quinolines by dehydrogenative annulation of amines and ketones are also performed.

To test this hypothesis, we designed and prepared a series of N-doped ordered mesoporous model carbon (designated as MNC-*x*; *x* = 316, 326, 336, 346, 359) catalysts with varying degrees of N-content and types of N-species using different precursors and we have thoroughly investigated their local structures and catalytic activities for BH reactions. Pristine mesoporous carbon matrices were prepared under nitrogen (designated as CMK-306) and argon (designated as CSI-306) atmospheres as control samples[41]. Further, we have also prepared nitrogen-containing carbons *via* a post-synthetic modification approach by treating pristine carbon samples with NH₃ to obtain CMK-306 (NH₃) and CSI-306 (NH₃), respectively.

EXPERIMENTAL DETAILS

Starting materials

All the chemicals used were of analytical grade. Benzyl alcohols, anilines, and their substituted analogs as well as other chemicals including tetraethyl orthosilicate, ethylenediamine ($\geq$ 99.5%), CCl_4 ($\geq$ 99.8%) melamine ($\geq$ 99.0%), *p*-phenylenediamine ($\geq$ 98.0%), acridine ($\geq$ 97.0%), *p*-diaminobenzene (98.0%), aniline (99.5%), pyrrole (99.1%), polyvinylpyrrolidone (PVP; 98.0%), phenanthridine ($\geq$ 99.0%), $CDCl_3$, and pluronic P-123 (Mol. Wt. 5800). KOH, Cs_2CO_3, toluene, HF (40% aqueous solution), HCl (36% aqueous solution), hexane, petroleum ether, ethyl acetate, and deuterated benzyl alcohol-α,α-d2 were obtained from various chemical resources, viz., Sigma-Aldrich, Tokyo Chemical Industries, Avra Chemicals, and SD-fine chemicals.

Materials Synthesis

Ordered Mesoporous Silica: The ordered mesoporous silica (OMS) such as SBA-15 was synthesized as per the literature reports [38,40,42,43]. In a typical synthesis of SBA-15 by hydrothermal method, 8.0 g of Pluronic P123 triblock copolymer, poly(ethylene glycol)-*b*-poly(propylene glycol)-*b*-poly(ethylene glycol) (average MW 5800) was dissolved in 60 g of Millipore water and 240 g of 2 M HCl by stirring at 35°C. Subsequently, 17.0 g of tetraethyl orthosilicate (TEOS) was added to the clear solution with further stirring at the same temperature for a period of 24 h. The final gel composition was 1 SiO_2 : 0.012 P123 : 6.5 HCl : 169 H_2O. The resulting mixture was aged at 100°C for 24 h and the obtained white solid was

collected by centrifugation, washed with copious water followed by ethanol washing, and then dried at 80ºC in air ambient inside a drying oven. The final product was calcined at 500°C for 6 h under an air atmosphere and thus obtained material was used as a silica template to prepare mesoporous pristine and nitrogenous carbons.

Ordered Mesoporous Carbons: For comparison, ordered mesoporous carbons (OMC), viz., CMK-306 and CSI-306 were also prepared according to the reported procedure[38,40,42,44]. In a typical synthesis, 1.0 g of SBA-15 silica template was added to a homogeneous solution containing 1.5 g sucrose in 4.0 mL of water and sonicated for 15 minutes to infiltrate the sucrose into the mesopores. Then 0.2 mL of H_2SO_4 (4 M) was added and further stirred for 1 h using a magnetic stirrer. The black suspension was dried at 80°C in a drying oven. The infiltration process is repeated for a second time by taking 0.8 g of sucrose in 1.5 mL of water and 0.1 mL of H_2SO_4 (4 M). Finally, the black dried powder was calcined at 600°C for 5 h under an argon atmosphere with a ramping temperature of 3°C/min. Then the silica/carbon composite was treated with a 5% HF solution to dissolve the silica template, washed thoroughly with copious water until the aqueous filtrate attains pH ~ 7, and finally dried at 80°C in a drying oven to obtain mesoporous CSI-306 carbon.   For the preparation of CMK-306, the carbonization step preparation was performed in a nitrogen atmosphere (100 mL/min.) instead of Argon at 600°C for a period of 5 h.

Mesoporous Nitrogenous Carbon: The N-doped mesoporous carbon model catalysts, viz., MNC-x (*x* = 316, 326, 336, 346, 356) were prepared using SBA-15 silica as a hard template by nano-casting method [38,40,42-46]. For the synthesis of MNC- *x*, in a 50 mL round-bottomed flask, the calcined SBA-15 (2.0 g) was dispersed in a suitable nitrogen-containing carbon precursor (*see* Table S1) and then stirred magnetically for 15 minutes at room temperature followed by sonication for another 30 min. The resultant mixture was further refluxed with continuous stirring at 90°C for 6 h. The dark brown-colored solid obtained was subsequently dried at 80°C in a drying oven. After ensuring complete dryness, the composite material was ground into a fine powder with a mortar and pestle. The powdered composite material was carbonized at 600°C (unless otherwise specified) for 5 h under an argon atmosphere (unless mentioned) with a ramping rate of 2°C/min. The MNC samples were recovered after the dissolution of the SBA-15 silica template with 5 wt% dilute HF and the sample was washed thoroughly with copious water until the aqueous filtrate attains pH ~ 7. Finally, the sample was washed with ethanol and dried at 80°C in a drying oven to obtain mesoporous carbon

(black powder). The N-doped carbons prepared using ethylenediamine, *p*-diaminobenzene, aniline, pyrrole, and PVP are represented as MNC-316, MNC-326, MNC-336, MNC-346. and MNC-356, respectively. Likewise, the simultaneous doping of nitrogen and oxygen in the carbon matrix is synthesized using PVP and is designated as MNC-356. The carbons prepared using ethylenediamine/PVP as a precursor and pyrolyzed at 700, 800, and 900°C are denoted as MNC-317/357, MNC-318/358, and MNC-319/359, respectively.

N-Modified Mesoporous Carbons: The pristine mesoporous CSI-306 and CMK-306 carbons obtained by the above method were post-synthetically modified by heating the sample under the flow of NH_3 gas at 900°C (100 mL/min.) for a period of 2 h. Then the sample was washed thoroughly with copious water until the aqueous filtrate attains pH ~ 7 and finally dried at 80°C in a drying oven to obtain CSI-306 (NH_3) and CMK-306 (NH_3).

N-Methyl Protected Nitrogenous Carbon: In a typical experiment, 0.5 g of MNC-316 catalyst was suspended in toluene solvent (10 mL) followed by the addition of 5 mmol of either methyl iodide (MeI) or benzyl iodide in a 25 mL RB flask. The entire content was stirred for 24 h at 70°C using a water condenser and oil-bath setup. After completion of the reaction, the content was washed thoroughly with water and ethanol and finally vacuum dried at 40°C in a vacuum oven to obtain N-methyl-protected nitrogenous carbon, i.e., MNC-316-MeI catalysts.

Mesoporous Carbon Nitride, g-C_3N_4. In a typical preparation of mesoporous *g*-C_3N_4, 5 g of melamine was dissolved in an equal amount of ethanol to obtain a homogeneous solution and then magnetically stirred for 15 min. after adding 2.0 g SBA-15 silica template[9,46,47]. The suspension was sonicated for 30 min. and then dried at 80°C in a drying oven for 12 h. The infiltration procedure was repeated for a second time using 3.0 g of melamine and the resulting melamine-silica composite particles were washed thoroughly with distilled water and ethanol followed by drying at 80°C in an oven. Then the thermal polymerization of melamine was performed at 600°C by heating under an argon atmosphere, at 2°C/min, using a tubular furnace. The polymerized sample was treated with 5 wt% dilute HF to dissolve the silica matrix and to obtain the mesoporous *g*-C_3N_4 with pale yellow color. The sample was washed thoroughly with copious water until the aqueous filtrate attains *p*H ~ 7 and dried in a drying oven at 80°C.

Materials characterization

Physico-Chemical Methods: All the synthesized ordered mesoporous carbons and nitrogen-doped ordered mesoporous carbon materials were carried out using a variety of techniques

which include X-ray diffraction (XRD), N_2 sorption measurements, elemental analysis, High-Resolution Transmission Electron Microscopy (HR-TEM), Scanning Electron Microscopy (SEM), Raman Spectroscopy, X-ray Photoelectron Spectroscopy (XPS), and ^{13}C solid-state nuclear magnetic resonance spectroscopy (^{13}C MAS-NMR).

XRD patterns of model catalysts were recorded using a Rigaku Miniflex II Diffractometer using Cu Kα radiation ($\lambda = 1.506$Å) equipped with a hybrid pixel array detector. The low-angle XRD patterns were collected in the 2θ range of 0.7 to 5 with a step size of 0.01º and step time of 2 s. TEM images were obtained by using a JEOL 2100 instrument at an accelerating voltage of 120 kV. A few milligrams of the test sample were dispersed in ethanol followed by sonication for 30 min and then cast onto a 200 mesh lacey foam-coated copper grid. Elemental analysis was performed using Perkin-Elmer 2400 series CHNS/O analyzer. Solid-state ^{13}C MAS-NMR spectra of samples were recorded on Bruker AV III HD Ascend 500MHz FT-NMR spectrometer at a spinning frequency of 8 kHz at room temperature using a 5 mm diameter ZrO_2 rotor. Nitrogen adsorption/desorption measurements were carried out on Micrometrics ASAP 2020 instrument. Prior to analysis, samples were degassed at 200°C for 10 h. The degassed samples were weighed and the nitrogen sorption measurements were carried out at a liquid nitrogen temperature of −196°C. The specific surface area was calculated by the BET method and the total pore volume was estimated from the nitrogen uptake at a relative pressure of $P/P_0 = 0.99$. The pore size distributions were calculated from the adsorption branch of the isotherm using the BJH method. XPS data were obtained with an Omicron Nanotechnology Spectrometer with a hemispherical analyzer using a monochromatic Al Kα (1486.6 eV) source operating at 15 kV and 20 mA. The electron binding energies (E_B) were obtained without charge compensation. For quantitative analysis, the peaks were deconvoluted with Gaussian-Lorentizian fits; the peak area was divided by a sensitivity factor obtained from the element-specific Scofield factor and the transmission function of the spectrometer. All the binding energy values reported here were corrected w.r.t. adventitious carbon (284.5 eV).

Reaction procedure

C-Alkylation of Anilines (Amines) with Benzyl Alcohol: In an oven dried 15 mL pressure tube Acetophenone (0.001 moles, 120 mg) was taken, to this benzylalcohol (0.0015 moles, 162 mg), catalyst MNC-316 (20 weight% with respect to Acetophenone, 24 mg), base t-BuOK (0.0003 moles, 33.6 mg) and Toluene (1 mL) added. After adding all these chemicals, Ar-gas flushed

for 1-2 minutes and then a PTFE cap was used to close the pressure tube. The reaction pressure tube was kept in 130ºC preheated silicon oil bath and stirred for 24 hours to complete the reaction. After completion, the reaction tube permitted to come to normal room temperature and then solid heterogeneous catalyst was separated by centrifugation and washed thoroughly with ethyl acetate. From the crude reaction mixture excess of solvent removed by using rotary evaporator and by using column chromatography (silica gel, hexanes/ethyl acetate) further purification done to get desired C-Alkylation product. Product structure was interpreted by ^{1}H-NMR, ^{13}C-NMR and HR-MS analysis.

N-Alkylation of Anilines (Amines) with Benzyl Alcohol: Aniline (1.5 Equiv.), benzyl alcohol (1.0 Equiv.), and magnetic stirring bar were transferred to a 15 mL quartz tube. Then 0.3 Equiv. KOH, 2 mL toluene, and 21 mg of pre-dried MNC–316 catalyst were added, and the tube reactor was gently flushed with argon for 5 min at room temperature and finally closed tightly with leak-proof glass joints. Then the quartz reactor was placed in a silicone oil bath preheated at 130°C (the reaction time was counted after immersing it for 15 minutes in order to attain the desired temperature) and the reaction mixture was magnetically stirred for a desired period of time. After completion of the reactions, the tube reactor was cooled down to ambient temperature; the solid catalyst was recovered by centrifugation and washed thoroughly with ethyl acetate. The yields were determined by isolation of compounds using column chromatography (silica gel column, hexane-ethyl acetate solvent system) for all substrate variation, whereas GC yield was considered for optimization of reaction conditions. After completing the reaction, dodecane (30 μL) as an external standard was added to the reaction mixture and then analyzed by GC equipped with a capillary column (OV-101), FID detector, and auto-sampler.

The C-alkylation of aromatic ketones was carried out using alcohols as an alkylating reagent in a tube reactor charged with inert gas at ambient pressure at a temperature ranging from 70-140 °C for a period of 1-24 h. After the addition of 5-50 wt% of heterogeneous heteroatom-doped catalysts with the reactants (aromatic ketones and alcohols) containing 0.1–0.6 equivalent to the appropriate base, the reaction was carried out by stirring magnetically in a preheated oil bath of specified temperature. After a period of 1-24 h of reaction period, the reaction mixture was analyzed by TLC using 5% ethyl acetate in a hexane solvent system. Finally, the pure products were isolated by column chromatography and confirmed by ^{1}H NMR, ^{13}C NMR, and mass spectroscopy.

Deuterium Labeling Study: In a typical deuterium labeling study, benzyl alcohol-α,α-d_2 (1.0 Equiv.) was mixed with aniline (1.5 Equiv.) in a 15 mL quartz tube. Then 0.3 Equiv. KOH, 2 mL toluene, and 21.6 mg of pre-dried MNC-316 catalyst were added to the tube reactor and gently flushed with argon for 5 min at room temperature, and finally closed tightly with leak-proof glass joints. Then the quartz reactor was placed in a silicone oil bath preheated at 130°C (the reaction time was counted after immersing it for 15 minutes in order to attain the desired temperature) and the reaction mixture was magnetically stirred for 16 h. After completion of the reactions, the tube reactor was cooled down to ambient temperature, the solid catalyst was recovered by centrifugation, and washed thoroughly with ethyl acetate. The yields were determined by isolation of compounds using column chromatography (silica gel column, hexane-ethyl acetate solvent system) and products were confirmed with ^{1}H NMR and HRMS spectra.

Kinetic Isotopic Study: For the kinetic isotopic effect (KIE) study, a mixture of benzyl alcohol-α,α-d_2, and normal benzyl alcohol in equimolar quantities (1.0 Equiv.) was reacted with aniline (1.5 Equiv.) and the reaction was performed under identical conditions. The reaction products were analyzed by ^{1}H-NMR and HRMS, and spectra are presented in supporting information (Tables S2 and S3). ^{1}H-NMR analysis exhibited a 47.0 % of 3aa, 41.0 % of H/D product (3aa-d_1) and 12.0 % of completely benzylic deuterated product (3aa-d_2). HRMS spectrum showed three peaks at 186.1, 185.1 and 184.1; the peak at 186.1 belongs to the compound 3aa-d_2 [$(C_{13}H_{11}D_2N + H)^+$], the peak at 185.1 belongs to 3aa-d_1 [$(C_{13}H_{12}DN + H)^+$] and the peak at 184.1 corresponds to 3aa [$(C_{13}H_{13}N + H)^+$]. From peak intensities, the percentages of 3aa, 3aa-d_1 and 3aa-d_2 were calculated as 47.0 %, 41.0 % and 12.0 %, respectively

Catalyst Recyclability: The recovered catalyst (MNC-316) from the first reaction run was washed thoroughly with ethanol and water successively and vacuum dried at 120°C to remove the occluded organic product or solvent molecules on the surface of catalysts. Then the standard N-alkylation reaction of aniline (1.5 Equiv.) with benzyl alcohol (1.0 Equiv.) was performed under identical conditions using a 15 mL quartz tube. As usual, the tube reactor was gently flushed with argon for 5 min at room temperature and tightly closed with leak-proof glass joints. After completion of the reactions, the tube reactor was cooled down to ambient temperature, the catalyst was recovered by centrifugation, washed with Millipore water and ethanol to remove the occluded product and solvent molecules at the end of the second cycle, and finally, vacuum-dried at 120°C in a vacuum oven. The entire process is essentially

repeated each time before commencing the next reaction run. The product yield was determined by the isolation of compounds using column chromatography (silica gel column, hexane-ethyl acetate solvent system). The recovered catalyst was again washed thoroughly, and all steps were essentially repeated for 6 consecutive reactions using the same catalyst.

Products analyses

Collection of ^{1}H NMR and ^{13}C NMR spectral data for product identification was made with Bruker BBFO (500 MHz & 400 MHz) spectrometer using CDCl$_3$ solvents. HRMS data were recorded on Agilent high-resolution mass spectrometer. GC analysis was performed on Agilent 7890B, equipped with a 30-meter capillary column (OV-101) fitted with a flame ionization detector (FID) and auto-sampler. Dodecane (30 μL) was used as an external standard for the quantification of products using GC. All catalytic experiments were carried out in a 15 mL sealed quartz tube (wall thickness of 3 *mm*) fitted with leak-proof toughened glass joint immersed in a silicone oil bath equipped with an inbuilt thermocouple to monitor temperature and sensor to control the stirring speed of the magnetic stirrer.

COMPUTATIONAL DETAILS

The calculations were performed employing the DFT code *Vienna Ab-initio Simulation Package* (VASP)[48], under the generalized gradient approximation (GGA) as proposed by Perdew, Burke, and Ernzerhof (PBE)[49]. A basis set of plane waves with an energy cutoff of 400 eV treats the valence electrons, whilst the inner electronic levels of the atoms are described with the projector-augmented-wave (PAW) method [50,51]. Long-range dispersion forces are included via Grimme's atomic pairwise method damped by the Becke-Johnson function[52–54]. The simulation cells have a dimension of more than 14 Å, thus only the Gamma point is used to sample the reciprocal space. The evaluation of the occupation of the electronic states and the integration over the reciprocal space is performed employing the Gaussian smearing method with a bandwidth of 0.05 eV[55,56]. During geometry optimization, convergence thresholds of 10^{-5} and 0.1 eV/Å control the electronic and ionic iterations, respectively. After geometry optimization, the structure of graphitic *g*-C$_3$N$_4$ is put through simulated annealing during 2.5 ps, from 0 to 130°C, to include the effects of temperature in the adsorption of potassium benzyl oxide.

We have used the nudged elastic band (NEB) method[57,58] to search for an initial guess of the transition state corresponding to the transfer of the hydride ion from benzyl oxide

to the N−doped carbon materials and g-C_3N_4. The resulting structure is then refined with the improved dimer method (IDM) using a convergence threshold for the ionic forces of 0.1 eV/Å. This procedure is applied to the single- and multi-layered N-doped and g-C_3N_4 systems[59]. In the case of multi-layered systems, the NEB calculation proceeds without constraints. However, due to the large number of atoms in the simulation cell, in the subsequent vibrational calculation that precedes the IDM calculation, only the layer with adsorbed potassium benzyl oxide is allowed to relax, whereas the rest of the material is kept frozen. The same constraints are applied during the IDM calculations. The optimized hexagonal unit cell of graphite yields values of 2.467 and 6.735 Å for the vectors a and c, respectively, with a C-C bond length and interlayer distance of 1.424 and 3.367 Å, respectively. These calculated lattice parameters are in good agreement with previous experimental and computational works[60,61]. The optimized values for the hexagonal unit cell of g-C_3N_4 are 7.130 and 6.288 Å for the vectors a and c, which compare well to previously calculated values of 7.11 and 6.13 Å (*see* Scheme S1-b)[62].

The simulation cells are prepared by expanding the orthorhombic unit cells of all-carbon graphite and graphitic g-C_3N_4 along with the three Cartesian directions (*see* Scheme S1-a, S1-b). In the case of pristine-carbon and N-doped graphite, an expansion of $6 \times 2 \times 3$ is used along the vectors a, b, and c, respectively, adding a vacuum gap of at least 20 Å along vector b to reproduce the edge of the material, which generates cells with a dimension of 14.8 $\times$ 32.3 $\times$ 19.4 Å^3 (*see* Scheme S1-c, S1-d). The same procedure is applied to g-C_3N_4, with an expansion of $2 \times 1 \times 3$, with a cell dimension of $14.2 \times 32.3 \times 17.6$ Å^3 (*see* Scheme S1-e). The edges are terminated with H atoms following a similar scheme as reported in the literature[63,64].

RESULTS AND DISCUSSION

As shown in Figure 2, the mesoscopic features are clear from low-angle XRD patterns (Figure 2A) and high-resolution TEM micrographs (Figure 2B). For comparison, we have also prepared nitrogen-rich g-C_3N_4 (57.8 % N) using a standard protocol based on melamine precursors. The mesostructure features, textural characteristics, and elemental composition of the catalysts were systematically confirmed by analytical (XRD, CHN), imaging (TEM) (*see* Figure 2, Table 1, and Figures S1 and S2), and spectroscopic (XPS, MAS-NMR) techniques. Figure 3A(a) depicts the core level N(1s) XP spectrum of g-C_3N_4 which displays a prominent

peak at 398.5 eV assigned to pyridinic-nitrogen (N4) of *tris-s*-triazine (*tris*−N) sub-units (Scheme 1b). The spectrum also indicates the presence of a small amount of graphitic nitrogen (*tris*−N/*grap*−N = 7) at 400.5 eV [31].

Figure 3A(*d-f*) depicts the core level N(1s) XP spectra of MNC- *x* samples with two main peaks centered at 398.0 and 400.1 eV, which are assigned to *pyri*−N (N1 and N2) and *grap*−N (N3), respectively [29] (*see* also Scheme 1a). In contrast, the control mesoporous carbon sample (CSI-306), carbonized under an argon atmosphere, shows no N (1s) signal (Figure 3A-*b*). Surprisingly, the second control sample, i.e., CMK-306, carbonized under a nitrogen atmosphere, exhibited a low N-content (1.8 %) and furnished primarily *pyri*−N at the edge/defect sites of the carbon matrix (*see* Figure 3A). Conversely, the ammonia-treated sample, CSI-306 (NH$_3$), had a higher N-content at 9.2 % albeit with considerable *pyri*−N (Figure 3A(*c*)). In the case of MNC-316 (N, 17.2 %), and MNC-326 (N, 18.1 %), with higher nitrogen content, both *pyri*−N and *grap*−N species appear in almost equal proportions, Figure 3A(*d-f*). Overall, the precursor method is more efficient in achieving a higher total N-content compared to post-functionalization. Additionally, the carbonization temperature is found to have a profound effect on the total nitrogen content as well as on the *pyri*−N/*grap*−N ratios. Upon increasing the carbonization temperature (600 to 900°C), we found a gradual reduction in the *pyri*−N species (398.0 eV), *see* Figure 3A(*f*) and Figure 4B.

The *g*-C$_3$N$_4$, MNC-316, and MNC-326 model catalysts were subjected to further investigation by ^{13}C MAS-NMR to identify the local environments around the nitrogen centers in the carbon matrix. The *g*-C$_3$N$_4$ with *tris*−N motif displays distinct narrow signals at 155 and 164 ppm, Figure 3B(*a*), corresponding to −CN$_3$ and −CN$_2$(NH$_x$), respectively [31]. Meanwhile, the ^{13}C-signal of CSI-306 (N is absent) shows a rather sharp resonance signal at 127 ppm analogous to graphite polymorph, Figure 2B(*b*). In contrast, the N-doped samples exhibited an intense signal centered at 127 ppm as expected, along with a broad signal at 145 ppm, Figure 3B(*c-f*). This additional peak has its origin in the local carbon environments affected by the adjoining nitrogen in these samples. The *pyri*−N species occurring at the edges/defects in an N-doped carbon matrix, as referred to in the literature are in effect benzannulated pyridines which can occur as acridinic (zig-zag) and phenanthridinic (arm-chair) sub-units, based on the local arrangement of the aromatic rings around the pyridine core. To confirm the existence of these substructures in our samples, we performed CP-MAS of pure phenanthridine and acridine. In the case of phenanthridine, a broad signal centered at 127 ppm along with two weak signals at 144 and 156 ppm were observed, Figure 3B(*g*). Likewise, pure

acridine furnished a strong signal at 127 ppm and two feeble signals at 140 and 151 ppm, Figure

3B(*h*). Therefore, the broad peak observed in our N-doped carbon samples centered around

145 ppm confirms the presence of benzannulated pyridinic local structures [32,33].

Additionally, these conclusions are supported by the deconvoluted XP spectra into

phenanthridine, acridine, and graphitic species with binding energy values of 398.0, 399.1, and

400.1 eV, respectively [29,30], *see* Figure 4A.   Figure 5 illustrates the N(1s) core level XP

spectra of various OMCs and MNCs including samples pyrolyzed under nitrogen atmosphere,

ammonia-treated, and samples carbonized using different organic precursors, viz.,

ethylenediamine (MNC-316), *p*-diaminobenzene (MNC-326), aniline (MNC-336) and pyrrole

(MNC-346).

      After establishing the local nitrogen substructures, we investigated the activity of a

model catalyst (MNC-316) for a standard borrowing-hydrogen type *N*-alkylation of aniline

with alcohols (Figure 6A). In an initial experiment with MNC-316 as a catalyst for the *N*-

alkylation of aniline using benzyl alcohol, we observed a substantial amount of the *N*-alkylated

products along with small amounts of imine. A control experiment with CSI-306, without

nitrogen in the carbon matrix, was found to be inactive in the BH reaction, indicating that the

presence of nitrogen is essential for the catalytic process. A second control in which the

nitrogen content of N-doped carbon was blocked by alkylation (treatment with MeI) led to a

drastic reduction in catalytic activity (*see* Table 1, Figure 4B). Furthermore, in order to

understand the catalytic role of carbon and KOH, a rigorous optimization of reaction conditions

was done using an MNC-316 catalyst. Initially, the effect of temperature was studied and the

resultant catalytic performance is shown in Table 3. The catalyst demonstrates apparent

conversion even at 100°C, but the product N-benzylaniline was obtained only at a temperature

of 130°C, below which probably the N-benzylanilide is formed. The effect of solvent on the

reaction progress, presented in Table 4, shows that among the various solvents when

dimethylsulphoxide and xylene were used, both the conversion and selectivity were poor as

compared with toluene. Remarkably, the reaction resulted in complete conversion without the

use of any solvent, possibly due to the effective interaction of the alcohol groups with the

inbuilt amine groups present in the catalyst. However, for effective mixing of the reactants,

toluene can be used for reactions with reactants having bulky groups.

      The reaction was carried out with different bases such as Cs_2CO_3, NaOH, and KOH,

and the results were presented in Table 4. When Cs_2CO_3 was used, the selectivity towards N-

benzylaniline was very poor (< 10%). Interestingly, when less than 0.3 Equiv. of KOH was

used as a base no product was seen, but 0.3 Equiv. was sufficient to achieve a conversion and product yield of greater than 90%. Beyond that, the addition of more KOH has very little effect on the reaction progress. At the same time, it is worth noting that simply using 0.3 Equiv. KOH has not resulted in any progress toward amine conversion. This can be seen in Table 4 wherein the effect of catalyst concentration is studied. The controlled blank reaction was performed using 0.3 Equiv. KOH and no catalyst have resulted in the scanty formation of amine product (*see* Table 4), confirming our N-doped carbon's catalytic activity. We have used different amounts of catalysts and we observed that 20 *mg* of catalyst is sufficient to achieve the maximum conversion. The reaction was also conducted under different atmospheres and it was observed that the yields in the presence of an O_2 atmosphere were less compared with an inert (argon) atmosphere as it is known that oxygen environments are detrimental to borrowing hydrogen reactions (*see* Table 5). In addition, the influence of reaction time and catalyst loading was also probed with **1a** and **3ca**, and the results are presented in Figures 7A and 7B. The figure shows that the complete conversion has taken place after 15 hours of reaction time. The final product amine started forming after 5 hours of reaction time, which means that the reaction will go through an intermediate form which is the imine. Benzyl alcohol is initially converted to aldehyde before the coupling reaction and reduction happen. Therefore, even though the conversion has finished within 15 h, the product formation has taken a longer reaction involving BH type of catalysis. With simple aniline and benzyl alcohol, the formation of benzyl aniline is seen to be complete in 10 h. Finally, the conditions used henceforth are as follows: alcohol (1 *mmol*), amine (1.5 *mmol*), catalyst 20 *wt%* of benzyl alcohol, KOH (0.3 *mmol*), solventless, temperature 130°C and reaction time 24 *h*, argon atmosphere. These optimized conditions were used in all further reactions.

Further, to demonstrate the synthetic utility of optimized N-doped carbon catalyst systems in BH *N*-alkylation reactions (Figure 6B), a variety of substituted aniline derivatives were reacted (**1a–1p**) with benzyl alcohol (**2**) under standard conditions to afford the corresponding *N*-alkylated products (**3**). Substrates bearing both electron-donating and electron-withdrawing functionalities, such as methoxy, *n*-butyl, and halogen substituents on the aryl ring of aniline, are well tolerated and readily gave *N*–monoalkylated anilines (**3aa–3pa**) in good yields (79-96%) (*see* Table S1 for NMR details). Also, reactions involving sterically hindered anilines like trimethoxy aniline (**3ea**), *o*-chloroaniline (**3ha**), and *o,m*-dichloroaniline (3ka) progressed smoothly and the corresponding *N*–monoalkylated products were isolated in good yields (79-97%). The reaction also proceeded smoothly with hetero-

aromatic amines to the corresponding products (3ma-3oa) in excellent yields (96-97%). Interestingly, a pharmaceutically important building block, aminobenzodioxane derivative (**3pa**), was also produced at 86% isolated yield. Next, we demonstrate the scope of various benzyl alcohols (**2a–2j**) with aniline (Figure 6C). Benzyl alcohols bearing substituents like methoxy, thiomethoxy, methyl, and chloro-functionalities (**2a–2j**) react smoothly with 1 to give the respective *N*-alkylated products (**3ab–3aj**) in excellent isolated yields (84-97%). Aliphatic alcohols like *n*-octanol also furnished good yields (86%), albeit at a slightly higher reaction temperature of 145°C (**3aj**). More importantly, the catalytic protocol is highly selective for monoalkylation and no dialkylated products were produced. Furthermore, the catalyst can be recycled for at least six successive cycles with a mere 8% loss in catalytic activity (Figure 8A). Since the reactant amount is not changed correspondingly, and/or no fresh catalyst is added to make up for the loss in the catalyst so as to compensate for this, the loss in activity during successive runs is attributed to the loss of the material during the catalyst recovery step and not due to any structural variation of the catalyst. Indeed, the characterization results of the spent catalyst, shown in Figures 8B (XRD) and 8C (TEM), clearly demonstrate that the mesostructured nature of the catalyst is well-retained.

To verify our hypothesis that phenanthridinic and acridinic substructures act as hydride shuttles in BH reactions, we correlated the initial activities of N-doped carbon catalysts, e.g., MNC-316, MNC-326, MNC-336, MNC-346, MNC-356, CMK-306, CSI-306 (NH_3) and CMK-306 (NH_3), with their *pyri*–N content. These catalysts have a total nitrogen content ranging from 2 to 18% (Table 1) with a *pyri*–N content of 1–9%. The catalytic activity of these model catalysts increases linearly with the *pyri*–N content (Figure 7C), which clearly indicates an important role for the benzannulated pyridinic structures in catalysis, in contrast to the catalytically inactive *grap*–N. In order to support this further, we have performed the reaction for the MNC catalysts carbonized at 900°C as well as N-modified OMCs carbonized at 900°C, e.g., MNC-319, MNC-329, MNC-339, MNC-349, MNC-359, CSI-309 and CSI-309(NH_3), and established that the *pyri*–N content is utmost important to obtain the desired product (Table 6). On the other hand, g-C_3N_4 with a very high N-content (57.8%) failed to catalyse the BH reaction, owing to an *s*-triazine core present (N4 sites), and this difference in activity clearly distinguishes the role of the *pyri*–N local substructure in NAD(P)H mimicking BH catalysis. Upon carbonization, precursors with single nitrogen atoms in the structure, *i.e.*, pyrrole and aniline, yield N-doped carbons with a lower pyridinic content (Table 1) which is in line with

the lower conversion observed with these catalysts under our standard *N*-alkylation conditions. Conversely, N-doped carbon samples obtained from precursors with two nitrogen atoms, i.e., ethylenediamine and *p*-diaminobenzene, show a higher edge pyridinic content and therefore a higher conversion (Table 1).

We have performed computer simulations based on the density functional theory (DFT) to support these findings. The overall catalytic process involves the transfer of two H atoms from benzyl alcohol to the carbon material, with the subsequent formation of benzaldehyde. The edge of the graphene-like sheet is expected to bind H atoms at successive stages of the reaction, with the first H arriving as a hydride H^- ion from potassium benzyl oxide forming benzaldehyde, and the second H transferred from water in a later stage as a proton (H^+), thereby re-forming potassium hydroxide. A similar mechanism has also been proposed for the amination of alcohols in carbon materials. We consider the initial hydride transfer critical, which is initiated by the adsorption of potassium benzyloxide at the edge of the material where N atoms are located with available lone pairs oriented parallel to the graphene sheet plane. Next, the catalytic activity of these model compounds such as phenanthridine and acridine as molecular catalysts in the benchmark *N*-alkylation of aniline was investigated under homogeneous conditions. The reaction with acridine, and phenanthridine (0.1 Equiv.) as catalysts produced 96%, and 90% of desired product, respectively, at 100% conversion. Thus, it is confirmed that N-containing polyaromatics like acridine and phenanthridine at the defect and edge sites of the carbon framework effectively promote the hydrogen shuttle in the borrowing-hydrogen cascade (Scheme S1).

We calculated the adsorption energies for different N-doped, all-carbon, and *g*-C$_3$N$_4$ models, represented by a truncated graphite structure with exposed edges terminated by H atoms as shown in Figure 9 (*a-g*) (details of the models used in this work are provided in the computational details section, and Scheme S2). The adsorption energy becomes more favorable with the number of doping N atoms, varying from −69 kJ/mol for one N atom to −154 kJ/mol for three N atoms. In contrast, the all-carbon material yields much weaker adsorption of −40 kJ/mol. Adsorption at the *g*-C$_3$N$_4$ is comparable to the N-doped structures, with −70 kJ/mol if the edge is terminated with H atoms and −152 kJ/mol if the edge of *g*-C$_3$N$_4$ is saturated instead with K atoms. Therefore, the strong adsorption of potassium benzyl oxide, as an initial requirement for the hydride transfer, can only be attained at the edge of the N-doped and *g*-C$_3$N$_4$ materials. These results are consistent with previous experimental and

computational reports on N-doped graphene, which highlight the importance of the interaction between potassium and nitrogen to enhance the potassium storage capacities of these materials[34,36,63,64]. However, the experiment shows that g-C_3N_4 is also unable to catalyze the amination reaction. The annealing of the H-terminated g-C_3N_4 system adsorbing potassium benzyl oxide shows that benzyl alcohol is re-formed after the transfer of one of the terminal H atoms from N as a proton to benzyl oxide, as shown by Figure 9(h). This process hampers the required H^- transfer and means that the edges of g-C_3N_4 will be covered by K^+ ions, forming a layer underneath benzyl oxide, as shown by Figure 9(i); the adsorption of potassium benzyl oxide is stronger on this K^+ layer. However, this has a negative impact on the kinetics of the potential H^- transfer. In the case of N-doped graphite and g-C_3N_4, we calculated the energy barriers for the transfer of the H^- ion, obtaining a value of $+55$ kJ/mol for this process when potassium benzyl oxide is adsorbed at the edge of N-doped graphite.

This activation energy is further reduced to $+14$ kJ/mol when it is calculated on N-doped graphene, which is a consequence of the additional steric effects in the multi-layered system compared to the single-layered one (*see* Figure 9(j, k)). In the case of a single layer of g-C_3N_4, we find a much higher barrier of $+110$ kJ/mol. We could not find the transition state for the multi-layered g-C_3N_4 with the edges coated with K^+ ions due to the structural strain imposed by the K^+ ions that do not allow the benzyl oxide to move closer to g-C_3N_4 in order for the H^- transfer to take place. Considering the trends observed for the N-doped material, the activation energy in multi-layered g-C_3N_4 should be much higher than $+100$ kJ/mol, which renders this process extremely improbable. Experimental reports have shown that harsh acidic treatment and the presence of transition metals are needed for the photocatalytic oxidation of benzyl alcohol using g-C_3N_4 [39,41]. These results highlight the thermodynamic and kinetic suitability of N-doped carbon to catalyze the amination reaction of alcohols in the presence of potassium hydroxide.

We have also analysed the co-doping of the carbon material with N and O atoms, with the O doping in the form of a carbonyl group. We have employed a single graphene layer to construct the models, as shown in Figure 10. When graphene is doped with a single *pyri*−N atom (Figures 10a1 and 10a2), the adsorption energy of potassium benzyl oxide on this site has a value of -56 kJ/mol, with an energy barrier for the transfer of the hydride ion to form benzaldehyde of $+29$ kJ/mol. If a carbonyl group is added to this system (Figures 10b1 and 10b2), in close proximity to the *pyri*−N, the strength of the adsorption increases, with a value

of −125 kJ/mol, due to the simultaneous interaction of the K^+ ion with the *pyri*−N and the carbonyl O sites. The energy barrier is also reduced by 7 kJ/mol, down to a value of + 22 kJ/mol. These variations are a result of the effective electron-withdrawing effects of the carbonyl group, which reduces the electron density of nearby C atoms belonging to the graphene sheet thereby facilitating the transfer of the hydride ion. This analysis is further supported by calculations carried out for a graphene sheet doped only with a carbonyl group (Figures 10c1 and 10c2), but this time transferring the H^- ion to a graphene C atom directly binding the carbonyl group. The electron-withdrawing effect is thus more noticeable during the H^- transfer, with an energy barrier as low as +12 kJ/mol, and adsorption energy that remains at approximately −100 kJ/mol. The addition of a *pyri*−N next to this carbonyl group (Figures 10d1 and 10d2) further enhances the capacity of the material to oxidize the benzyl oxide molecule, now showing an adsorption energy of −141 kJ/mol, and the lowest barrier calculated in the present work for the transfer of the hydride ion, with a value of only +5 kJ/mol. But, if instead of a *pyri*−N, a *grap*−N atom binds the carbonyl forming an amide group (Figures 10e1 and 10e2), the adsorption of potassium benzyl oxide is weaker compared to the system without N doping, with an adsorption energy of −68 kJ/mol, but more importantly, the energy barrier for the hydride transfer increases by a factor of 3, from +12 to +40 kJ/mol. The negative impact of *grap*−N can be explained if we consider that this type of doping places the nitrogen's lone pair in a *p*-orbital perpendicular to the graphene sheet, which is directly engaged in the π conjugation and thus has the electron-donating capability. Therefore, *grap*−N tends to cancel out the favourable action of the carbonyl group on the oxidation of benzyl oxide. These outcomes show that a cooperative effect can be achieved by co-doping the material with N and O in the form of pyridinic and carbonyl sites, respectively. This co-doping enhances the efficiency of the material to adsorb potassium benzyl oxide through the simultaneous interaction of K^+ with the N and O's lone pairs, while the electron-withdrawing effect of the carbonyl group increases the efficiency of the hydride transfer from benzyl oxide to the carbon material. However, the proximity between *pyri*−N and carbonyl sites in the actual material may not always be ideal, and the occurrence of the O doping as carbonyl groups may also be hampered and hence the activity (MNC-356, Table 1), which would hinder the effectiveness of the discussed synergy in the co-doped carbons.

To confirm the mechanism of the BH cascade, we undertook preliminary mechanistic studies using deuterated benzyl alcohol-α,α-d2. To prove that the benzyl alcohol acts as a generic hydride source, we allowed the benzyl alcohol-α,α-d2 (**1a−d2**) to react with aniline (**2a**)

19

under optimized reaction conditions. We analyzed the product distribution by ^{1}H NMR and HRMS which revealed 43.1% incorporation of deuterium at the benzylic position of **3aa−d₁** (Table 7 and Table S2). This deuterium incorporation supports a borrowing-hydrogen mechanism and agrees with earlier reports [65,66]. Furthermore, kinetic isotopic effect (KIE) studies were performed to gain more insight into the reaction mechanism under the optimized reaction conditions. Accordingly, one of the two C−D bonds needs to be broken in order for the reaction to take place. Further, in parallel experiments performed by our group with simple benzylalcohol and with α,α-d2 benzylalcohol, we observed that the D/H exchange product in case of α,α-d2 benzylalcohol. This also demonstrates that only one of the two C−D bonds needs to be broken and these results prove that the reaction under discussion follows the borrowing hydrogen mechanism. We observed a $k_{CHH}/k_{CDH} = 1.15$ based on ^{1}H NMR and HRMS (Table 8 and Table S3), which suggests the participation of a benzylic C–H bond in the borrowing hydrogen cascade. The hydride transfer pathway as depicted in Figure 11 is initiated by a base-assisted dehydrogenation of the alcohol, forming a proposed dihydro-derivative at the benzanulated (dihydro- not shown in Figure 11, add 2 H atoms) pyridine local substructures in the N-doped carbon matrix. The resulting carbonyl compound forms an imine which is subsequently hydrogenated by the local dihydro-structure in a NAD(P)H mimicking step to form the final amine product[33]. As seen in Figure 11, for *N*-benzylation of aniline, the present catalytic system (MNC-316) demonstrates consistent activity and stability. The current catalytic protocol can be scaled-up to a gram scale with a minimal decrease in yield (**3aa**).

On the other hand, nitrogen heterocycles are abundant in nature and constitute the backbone of numerous organic functional materials, natural products, and pharmaceutically important molecules. The quinoline moiety is present in many classes of biologically active compounds and is one of the most popular N-heteroaromatics incorporated into the structure of many pharmaceuticals. Quinoline and its derivatives exhibit a wide spectrum of pharmacological activities such as antifungal, antimalarial, anti-inflammatory, antioxidant, antileishmanial, anthelmintic, anticonvulsant, antitumor, antiplatelet, cardiotonic, antimicrobial, and antibacterial agents. In addition, they function as pharmacologically active synthetic compounds, e.g., with deoxyribonucleic acid (DNA) binding capabilities and with DNA-intercalating carriers. Thus, the N-doped carbon developed herein can also be used as novel heterogeneous catalysts for the following organic transformations: *N*-alkylation of amines using alcohols; *C*–alkylation of ketones using alcohols; synthesis of quinolines by dehydrogenative condensation reactions between amino alcohols and ketones. *C*–alkylation

of ketones was carried out using model reactions represented in Figure 12 **(6aa–6ad)**, and the synthesis of quinolines was performed using 2-amino benzyl alcohols and methyl ketones (Figure 13; **9aa, 9ab**). Both these model reactions and analogous substrate scope resulted in yields up to 97% (*cf.* Figures 12 and 13; see Table S1 for NMR details) under optimized conditions, demonstrating the wide capability of the *Pyri*–N substituted metal-free carbons in catalyzing BH reactions.

CONCLUSION

We have developed efficient heterogeneous N-doped mesoporous carbon materials which successfully catalysed direct N– alkylation and C–alkylation reactions with alcohols via borrowing-hydrogen or hydrogen auto-transfer. In this investigation, we have demonstrated that the local benzannulated pyridine sub-units present in the edges/defects of N-doped carbons act as exceptionally efficient hydride shuttles in metal-free biomimetic borrowing hydrogen cascades, i.e., for heterogeneous direct N– alkylation and C–alkylation of anilines and ketones employing alcohols under hydrogen auto-transfer conditions. The critical role of the local substructures in N-doped carbons in catalysis is highlighted by the lack of catalytic activity of g-C_3N_4 despite its high nitrogen content. This study establishes the crucial parameters required for the synthesis of N-doped carbons with high pyridinic content for efficient catalysis. Furthermore, we have also established the utility of this transformation in the synthesis of highly valuable quinoline systems. Deuterium-labelling studies have confirmed that the present reaction proceeds through the hydrogen auto-transfer pathway.   In addition, this investigation will also pave the way for the design and development of robust carbon-based catalysts with fine-tuned functionalities.

SUPPORTING INFORMATION

Physico-chemical characterization data of catalyst and reaction products including original spectra are provided in the form of schemes, figures, and tables.

AUTHOR INFORMATION

Corresponding Author: Tel.: + 91-44-2257-4235; E-mail: selvam@iitm.ac.in (P. Selvam)

CONFLICT OF INTEREST: The authors declare no conflict of interest.

ACKNOWLEDGMENT

AUTHOR CONTRIBUTIONS

VTB conceived the project. PS and MS designed and developed the catalysts. PS, MS, VTB, and KN planned the experiments and supervised the project. TVRM synthesized and characterized the catalysts, MN conducted the catalytic experiments and characterized the products, and KK prepared the catalyst and conducted the catalytic experiments. PS, MS, VTB, NHdL, and CEHT planned the modeling studies and CEHT performed the calculations. NHdL commented on the manuscript writing and the result discussion.

REFERENCES

[1]   A. Roucoux, J. Schulz, H. Patin, Reduced transition metal colloids: A novel family of reusable catalysts? Chem Rev. 102 (2002) 3757–3778. https://doi.org/10.1021/cr010350j.

[2]   L. Ackermann, R. Vicente, A.R. Kapdi, Transition-metal-catalyzed direct arylation of (hetero)arenes by C-H bond cleavage, Angew. Chem. Int. Ed. 48 (2009) 9792–9826. https://doi.org/10.1002/anie.200902996.

[3]   D.S. Su, S. Perathoner, G. Centi, Nanocarbons for the development of advanced catalysts, Chem Rev. 113 (2013) 5782–5816. https://doi.org/10.1021/cr300367d.

[4]   X. Liu, L. Dai, Carbon-based metal-free catalysts, Nat Rev Mater. 1 (2016). https://doi.org/10.1038/natrevmats.2016.64.

[5]   S. Navalon, A. Dhakshinamoorthy, M. Alvaro, M. Antonietti, H. García, Active sites on graphene-based materials as metal-free catalysts, Chem Soc Rev. 46 (2017) 4501–4529. https://doi.org/10.1039/c7cs00156h.

[6]   L. Liu, Y.P. Zhu, M. Su, Z.Y. Yuan, Metal-Free Carbonaceous Materials as Promising Heterogeneous Catalysts, ChemCatChem. 7 (2015) 2765–2787. https://doi.org/10.1002/cctc.201500350.

[7]   Z. Yang, Z. Liu, H. Zhang, B. Yu, Y. Zhao, H. Wang, G. Ji, Y. Chen, X. Liu, Z. Liu, N-Doped porous carbon nanotubes: Synthesis and application in catalysis, Chem. Comm. 53 (2017) 929–932. https://doi.org/10.1039/c6cc09374d.

[8]   H. Yang, X. Cui, X. Dai, Y. Deng, F. Shi, Carbon-catalysed reductive hydrogen atom transfer reactions, Nat Commun. 6 (2015) 6478. https://doi.org/10.1038/ncomms7478.

[9]   F. Goettmann, A. Fischer, M. Antonietti, A. Thomas, Chemical synthesis of mesoporous carbon nitrides using hard templates and their use as a metal-free catalyst for Friedel-Crafts reaction of benzene, Angew. Chem. Int. Ed. 45 (2006) 4467–4471. https://doi.org/10.1002/anie.200600412.

[10] D. Guo, R. Shibuya, C. Akiba, S. Saji, T. Kondo, J. Nakamura, Active sites of nitrogen-doped carbon materials for oxygen reduction reaction clarified using model catalysts, Science. 351 (2016) 361-365. https://doi.org/10.1126/science.aad0832.

[11] C. Gunanathan, D. Milstein, Applications of acceptorless dehydrogenation and related transformations in chemical synthesis, Science. 341 (2013) 1229712. https://doi.org/10.1126/science.1229712.

[12] Q. Yang, Q. Wang, Z. Yu, Substitution of alcohols by N-nucleophiles via transition metal-catalyzed dehydrogenation, Chem Soc Rev. 44 (2015) 2305–2329. https://doi.org/10.1039/c4cs00496e.

[13] A.J.A. Watson, J.M.J. Williams, The give and take of alcohol activation, Science. 329 (2010) 635-636. https://doi.org/10.1126/science.1191843.

[14] F. Huang, Z. Liu, Z. Yu, C-alkylation of ketones and related compounds by alcohols: Transition-metal-catalyzed dehydrogenation, Angew. Chem. Int. Ed. 55 (2016) 862-875. https://doi.org/10.1002/anie.201507521.

[15] G.E. Dobereiner, R.H. Crabtree, Dehydrogenation as a substrate-activating strategy in homogeneous transition-metal catalysis, Chem Rev. 110 (2010) 681–703. https://doi.org/10.1021/cr900202j.

[16] J.M. Ketcham, I. Shin, T.P. Montgomery, M.J. Krische, Catalytic enantioselective C-H functionalization of alcohols by redox-triggered carbonyl addition: Borrowing hydrogen, returning carbon, Angew. Chem. Int. Ed. 53 (2014) 9142–9150. https://doi.org/10.1002/anie.201403873.

[17] M.G. Edwards, R.F.R. Jazzar, B.M. Paine, D.J. Shermer, M.K. Whittlesey, J.M.J. Williams, D.D. Edney, Borrowing hydrogen: a catalytic route to C–C bond formation from alcohols, Chem. Comm. 4 (2004) 90–91. https://doi.org/10.1039/b312162c.

[18] Y. Zhang, C.S. Lim, D.S. Boon Sim, H.J. Pan, Y. Zhao, Catalytic enantioselective amination of alcohols by the use of borrowing hydrogen methodology: Cooperative catalysis by iridium and a chiral phosphoric acid, Angew. Chem. Int. Ed. 53 (2014) 1399–1403. https://doi.org/10.1002/anie.201307789.

[19] D. Shen, D.L. Poole, C.C. Shotton, A.F. Kornahrens, M.P. Healy, T.J. Donohoe, Hydrogen-borrowing and interrupted-hydrogen-borrowing reactions of ketones and methanol catalyzed by iridium, Angew. Chem. Int. Ed. 54 (2015) 1642–1645. https://doi.org/10.1002/anie.201410391.

[20] S. Elangovan, J. Neumann, J.B. Sortais, K. Junge, C. Darcel, M. Beller, Efficient and selective N-alkylation of amines with alcohols catalysed by manganese pincer complexes, Nat Commun. 7 (2016) 12641. https://doi.org/10.1038/ncomms12641.

[21] N. Deibl, R. Kempe, Manganese-Catalyzed Multicomponent Synthesis of Pyrimidines from Alcohols and Amidines, Angew. Chem. Int. Ed. 56 (2017) 1663-1666. https://doi.org/10.1002/anie.201611318.

[22] T. Yan, B.L. Feringa, K. Barta, Iron catalysed direct alkylation of amines with alcohols, Nat Commun. 5 (2014) 5602. https://doi.org/10.1038/ncomms6602.

[23] S. Elangovan, J.-B. Sortais, M. Beller, C. Darcel, Iron-Catalyzed α-Alkylation of Ketones with Alcohols, Angew. Chem. 127 (2015) 14691–14694. https://doi.org/10.1002/ange.201506698.

[24] S. Rösler, M. Ertl, T. Irrgang, R. Kempe, R. Cobalt-Catalyzed Alkylation of Aromatic Amines by Alcohols. Angew. Chem. Int. Ed. 127 (2015) 15260–15264. https://doi.org/10.1002/ange.201507955.

[25] J.R. Frost, C.B. Cheong, W.M. Akhtar, D.F.J. Caputo, N.G. Stevenson, T.J. Donohoe, Strategic Application and Transformation of ortho-Disubstituted Phenyl and Cyclopropyl Ketones to Expand the Scope of Hydrogen Borrowing Catalysis, J Am Chem Soc. 137 (2015) 15664–15667. https://doi.org/10.1021/jacs.5b11196.

[26] M.L. Buil, M.A. Esteruelas, J. Herrero, S. Izquierdo, I.M. Pastor, M. Yus, Osmium catalyst for the borrowing hydrogen methodology: α-alkylation of arylacetonitriles and methyl ketones, ACS Catal. 3 (2013) 2072–2075. https://doi.org/10.1021/cs4005375.

[27] A. Corma, J. Navas, M.J. Sabater, Advances in One-Pot Synthesis through Borrowing Hydrogen Catalysis, Chem Rev. 118 (2018) 1410–1459. https://doi.org/10.1021/acs.chemrev.7b00340.

[28] K.I. Shimizu, Heterogeneous catalysis for the direct synthesis of chemicals by borrowing hydrogen methodology, Catal Sci Technol. 5 (2015) 1412–1427. https://doi.org/10.1039/c4cy01170h.

[29] W.J. Gammon, O. Kraft, A.C. Reilly, B.C. Holloway, Experimental comparison of N(1s) X-ray photoelectron spectroscopy binding energies of hard and elastic amorphous carbon nitride films with reference organic compounds, Carbon. 41 (2003) 1917-1923. https://doi.org/10.1016/S0008-6223(03)00170-2.

[30] K.D. Bartle, D.L. Perry, S. Wallace, The functionality of nitrogen in coal and derived liquids: An XPS study, Fuel Process. Technol. 15 (1987) 351-361. https://doi.org/10.1016/0378-3820(87)90057-9.

[31] J. Sun, J. Zhang, M. Zhang, M. Antonietti, X. Fu, X. Wang, Bioinspired hollow semiconductor nanospheres as photosynthetic nanoparticles, Nat Commun. 3 (2012) 1139. https://doi.org/10.1038/ncomms2152.

[32] F.G. Mutti, T. Knaus, N.S. Scrutton, M. Breuer, N.J. Turner, Conversion of alcohols to enantiopure amines through dual-enzyme hydrogen-borrowing cascades, Science. 349 (2015) 1525-1529. https://doi.org/10.1126/science.aac9283.

[33] Q.A. Chen, K. Gao, Y. Duan, Z.S. Ye, L. Shi, Y. Yang, Y.G. Zhou, Dihydrophenanthridine: A new and easily regenerable NAD(P)H model for biomimetic asymmetric hydrogenation, J Am Chem Soc. 134 (2012) 2442–2448. https://doi.org/10.1021/ja211684v.

[34] F.M. Hassan, V. Chabot, J. Li, B.K. Kim, L. Ricardez-Sandoval, A. Yu, Pyrrolic-structure enriched nitrogen doped graphene for highly efficient next generation supercapacitors, J Mater Chem A Mater. 1 (2013) 2904–2912. https://doi.org/10.1039/c2ta01064j.

[35] P. Selvam, T.V.R. Mohan, M. Sasidharan, V.T. Bhat, K. Namitharan, N. Madhu, K. Kala, Method for Using Bulk and Porous N-containing/N-doped Carbon and Carbon Nitrides as Heterogeneous Catalysts for Borrowing Hydrogen and Dehydrogenation Reactions., International patent WO/2020/016908, (2019).

[36] K. Share, A.P. Cohn, R. Carter, B. Rogers, C.L. Pint, Role of Nitrogen-Doped Graphene for Improved High-Capacity Potassium Ion Battery Anodes, ACS Nano. 10 (2016) 9738–9744. https://doi.org/10.1021/acsnano.6b05998.

[37] P. Selvam, T.V.R. Mohan, Application of metal-free ordered mesoporous nitrogenous carbons as electrocatalysts for oxygen reduction reaction and thereof, Indian patent 410837, (2022).

[38] T.V.R. Mohan, S. Palla, B. Kuppan, N.S. Kaisare, P. Selvam, Hydrogen Sorption Characteristics of Ordered Mesoporous Carbons: Experimental and Modeling View Point, J Chem Eng Data. 63 (2018) 4543–4551. https://doi.org/10.1021/acs.jced.8b00627.

[39] Z. Ju, P. Li, G. Ma, Z. Xing, Q. Zhuang, Y. Qian, Few layer nitrogen-doped graphene with highly reversible potassium storage, Energy Storage Mater. 11 (2018) 38–46. https://doi.org/10.1016/j.ensm.2017.09.009.

[40] T.V.R. Mohan, B. Kuppan, P. Selvam, Ordered nanostructured carbons, NCCR-41 and CMK-3: Synthesis, characterization, and hydrogen sorption studies, Catalysis in Green Chemistry and Engineering. 1 (2018) 1-12.

[41] P. Chen, J.J. Yang, S.S. Li, Z. Wang, T.Y. Xiao, Y.H. Qian, S.H. Yu, Hydrothermal synthesis of macroscopic nitrogen-doped graphene hydrogels for ultrafast supercapacitor, Nano Energy. 2 (2013) 249–256. https://doi.org/10.1016/j.nanoen.2012.09.003.

[42] T.V. Rama Mohan, P. Sridhar, P. Selvam, Experimental and modelling studies of carbon dioxide capture onto pristine, nitrogen-doped, and activated ordered mesoporous carbons, RSC Adv. 13 (2023) 973–989. https://doi.org/10.1039/D2RA07171A.

[43] D. Zhao, Q. Huo, J. Feng, B.F. Chmelka, G.D. Stucky, Nonionic triblock and star diblock copolymer and oligomeric sufactant syntheses of highly ordered, hydrothermally stable, mesoporous silica structures, J Am Chem Soc. 120 (1998) 6024-6036. https://doi.org/10.1021/ja974025i.

[44] S. Jun, Sang Hoon Joo, R. Ryoo, M. Kruk, M. Jaroniec, Z. Liu, T. Ohsuna, O. Terasaki, Synthesis of new, nanoporous carbon with hexagonally ordered mesostructure, J Am Chem Soc. 122 (2000) 10712-10713. https://doi.org/10.1021/ja002261e.

[45] F. Schüth, Non-siliceous mesostructured and mesoporous materials, Chem. Mat. 13 (2001) 3184-3195. https://doi.org/10.1021/cm011030j.

[46] A. Vinu, Two-dimensional hexagonally-ordered mesoporous carbon nitrides with tunable pore diameter, surface area and nitrogen content, Adv Funct Mater. 18 (2008) 816-827. https://doi.org/10.1002/adfm.200700783.

[47] M. Groenewolt, M. Antonietti, Synthesis of g-C3N4 nanoparticles in mesoporous silica host matrices, Adv. Mater. 17 (2005) 1789–1792. https://doi.org/10.1002/adma.200401756.

[48] G. Kresse, J. Hafner, Ab initio molecular-dynamics simulation of the liquid-metalamorphous- semiconductor transition in germanium, Phys Rev B. 49 (1994). https://doi.org/10.1103/PhysRevB.49.14251.

[49] G. Kresse, J. Furthmüller, Kresse, G., Furthmüller, J. (1996). Efficient iterative schemes for ab initio total-energy calculations using a plane-wave basis set. Phys Rev B. 54 (1996) 11169–11186. http://link.aps.org/doi/10.1103/PhysRevB.54.1.

[50] J.P. Perdew, K. Burke, M. Ernzerhof, Generalized Gradient Approximation Made Simple [Phys. Rev. Lett. 77, 3865 (1996)], Phys Rev Lett. 78 (1997). https://doi.org/10.1103/physrevlett.78.1396.

[51] P.E. Blochl, Projector augmented-wave method, Phys Rev B. 50 (1994) 17953–17979.

[52] S. Grimme, Semiempirical GGA-type density functional constructed with a long-range dispersion correction, J Comput Chem. 27 (2006) 1787–1799. https://doi.org/10.1002/jcc.20495.

[53] G. Kresse, D. Joubert, From ultrasoft pseudopotentials to the projector augmented-wave method, Phys Rev B. 59 (1999) 1758–1775.

[54] M. Hermann, R. Wu, D.C. Grenz, D. Kratzert, H. Li, B. Esser, Thioether- and sulfone-functionalized dibenzopentalenes as n-channel semiconductors for organic field-effect transistors, J Mater Chem C. 6 (2018) 5420-5426. https://doi.org/10.1039/c8tc00970h.

[55] S. Grimme, S. Ehrlich, L. Goerigk, Effect of the damping function in dispersion corrected density functional theory, J Comput Chem. 32 (2011) 1456–1465. https://doi.org/10.1002/jcc.21759.

[56] K.M. Ho, C.L. Fu, B.N. Harmon, W. Weber, D.R. Hamann, Vibrational frequencies and structural properties of transition metals via total-energy calculations, Phys Rev Lett. 49 (1982) 673-676. https://doi.org/10.1103/PhysRevLett.49.673.

[57] C.-L. Fu, K.-M. Ho, First-principles calculation of the equilibrium ground-state properties of transition metals: Applications to Nb and Mo, Phys Rev B. 28 (1983) 5480–5486.

[58] G. Mills, H. Jónsson, G.K. Schenter, Reversible work transition state theory: application to dissociative adsorption of hydrogen, Surf. Sci. 324 (1995) 305–337. doi.org/10.1016/0039-6028(94)00731-4

[59] H. Jónsson, G. Mills, K.W. Jacobsen, Nudged elastic band method for finding minimum energy paths of transitions. In Classical and Quantum Dynamics in Condensed Phase Simulations, World Scientific, (1998) 385–404. https://doi.org/10.1142/9789812839664_0016.

[60] A. Heyden, A.T. Bell, F.J. Keil, Efficient methods for finding transition states in chemical reactions: Comparison of improved dimer method and partitioned rational function optimization method, J. Chem. Phy. 123 (2005) 224101. https://doi.org/10.1063/1.2104507.

[61] P. Trucano, R. Chen, Structure of graphite by neutron diffraction, Nature. 258 (1975) 136-137. https://doi.org/10.1038/258136a0.

[62] P. v. Avramov, S. Sakai, S. Entani, Y. Matsumoto, H. Naramoto, Ab initio LC-DFT study of graphene, multilayer graphenes and graphite, Chem Phys Lett. 508 (2011) 86–89. https://doi.org/10.1016/j.cplett.2011.04.016.

[63] T. Xiong, W. Cen, Y. Zhang, F. Dong, Bridging the g-C_3N_4 Interlayers for Enhanced Photocatalysis, ACS Catal. 6 (2016) 2462–2472. https://doi.org/10.1021/acscatal.5b02922.

[64] C.S. Wu, J. da Chai, Electronic properties of zigzag graphene nanoribbons studied by TAO-DFT, J Chem Theory Comput. 11 (2015) 2003–2011. https://doi.org/10.1021/ct500999m.

[65] L. Zhang, D. Liu, J. Guan, X. Chen, X. Guo, F. Zhao, T. Hou, X. Mu, Metal-free g-C$_3$N$_4$ photocatalyst by sulfuric acid activation for selective aerobic oxidation of benzyl alcohol under visible light, Mater Res Bull. 59 (2014) 84–92. https://doi.org/10.1016/j.materresbull.2014.06.021.

[66] M.J. Lima, P.B. Tavares, A.M.T. Silva, C.G. Silva, J.L. Faria, Selective photocatalytic oxidation of benzyl alcohol to benzaldehyde by using metal-loaded g-C3N4 photocatalysts, Catal Today. 287 (2017) 70–77. https://doi.org/10.1016/j.cattod.2016.11.023.

Table 1. Textural properties and reactivity of N-doped mesoporous carbon catalysts for alcohol amination reaction.[a,b]

Catalyst	C & N Source	S_{BET} (m^2g^{-1})	V_P (cm^3g^{-1})	D_{BJH} (nm)	N-content (%) CHN	N-content (%) XPS	Alcohol conversion (%)	Product selectivity (%) Amine	Product selectivity (%) Imine
MNC-316	EDA	571	0.74	3.9	17.2	17.7	> 99 (98)[c]	> 99 (98)[c]	< 1 (2)[c]
MNC-316(MeI)	EDA	368	0.34	3.7	17.2	17.7	26[d]	19	7
No Catalyst	---	---	---	---	---	--	32[d]	13	19
No Base	EDA	571	0.74	3.9	17.2	17.7	---	---	---
MNC-326	*p*-DAB	436	0.42	3.8	18.1	17.8	> 99	> 99	< 1
MNC-336	Aniline	458	0.38	3.1	13.8	10.9	94	93	1
MNC-346	Pyrrole	603	0.46	3.4	12.5	12.4	90	89	1
MNC-356	PVP	561	0.62	3.8	7.7	6.7	85	80	19
CMK-306	Sucrose	637	0.47	3.4	1.8	2.4	18[d]	9	3
CMK-306(NH_3)	Sucrose	1138	0.91	3.9	7.8	6.1	32[d]	19	13
g-C_3N_4	Melamine	63	0.12	3.5	57.6	57.2	< 1	---	---

[a] General reaction conditions: Benzyl alcohol (1 *mmol*); Aniline (1.5 *mmol*); Catalyst (20 wt% of benzyl alcohol); KOH (0.3 *mmol*); Solvent (toluene; 1 *mL*); Temperature (130°C); Time (18 *h*); Atmosphere (argon). EDA: Ethylene diamine; *p*-DAB: *para*-Diaminobenzene. [b] Substrate and product selectivity were determined by GC-FID using dodecanol as the external standard; the reactions were repeated two times and the average results are provided. [c] Data after 7 recycles. [d] The remaining conversion is associated with the formation of phenylmethanolate as another product.

Table 2. Effect of reaction temperature with MNC-316 catalyst.[a,b]

Temperature, °C	Alcohol conversion, %	Product distribution, %	
		Amine	Imine
140	100	99	1
130	100	99	1
120	91	96	4
110	81	95	5
100	68	95	5

[a] General reaction conditions: Benzyl alcohol, 1 mmol; Aniline, 1.5 mmol; KOH, 0.3 mmol; Time, 18 h; Catalyst, 20 wt% of benzyl alcohol; Solvent (toluene; 1 mL); Atmosphere (argon).

[b] Substrate and product selectivity were determined by GC-FID using dodecanol as the external standard. The reactions were repeated two times and the average results are provided.

Table 3. Effect of solvents with MNC-316 catalyst.[a,b]

Solvent	Quantity, mL	Alcohol conversion, %	Product distribution, %	
			Amine	Imine
Toluene	2.0	93	97	3
	1.0	96	98	2
m-Xylene	2.0	90	98	2
DMSO	2.0	71	97	3

[a] General reaction conditions: Benzyl alcohol, 1 mmol; Aniline, 1.5 mmol; KOH, 0.3 mmol; Temperature, 130°C; Time, 18 h; Catalyst, 20 wt% of benzyl alcohol; Atmosphere, argon.

[b] Substrate and product selectivity were determined by GC-FID using dodecanol as the external standard. The reactions were repeated two times and the average results are provided.

Table 4. Optimization of base concentration with MNC-316 catalyst.[a,b]

Base	Quantity, *Equiv.*	Alcohol conversion, %	Product distribution, %	
			Amine	Imine
No base	---	--	--	--
No catalyst	0.3	32	13	19
KOH	0.1	43	42	1
	0.3	> 99	99	1
NaOH	0.3	61	60	1
Cs$_2$CO$_3$	0.3	13	12	1

[a] General reaction conditions: Benzyl alcohol, 1 mmol; Aniline, 1.5 mmol; Temperature, 130°C; Time, 18 h; Catalyst, 20 wt% of benzyl alcohol; Solvent (toluene), 1 mL; Atmosphere, argon.

[b] Substrate and product selectivity were determined by GC-FID using dodecanol as the external standard. The reactions were repeated two times and the average results are provided.

Table 5. Influence of reaction atmosphere with MNC-316 catalyst.[a,b]

Atmosphere	Alcohol conversion, %	Product distribution, %	
		Amine	Imine
Argon	> 99.0	99.0	1.0
Air	94.6	52.1	42.5
O_2 (in pressure tube)	97.2	--	97.2
O_2 (in a balloon)	90.8	60.5	30.3

[a] General reaction conditions: Benzyl alcohol, 1 mmol; Aniline, 1.5 mmol; KOH, 0.3 mmol; Temperature, 130°C; Time, 18 h; Catalyst, 20 wt% of benzyl alcohol; Solvent (toluene), 1 mL).

[b] Substrate and product selectivity were determined by GC-FID using dodecanol as the external standard. The reactions were repeated two times and the average results are provided.

5

Table 6. Effect of carburization temperature of the catalyst.[a,b]

Catalyst	Pyrolysis Temperature, °C	Alcohol conversion, %	Product distribution, %	
			Amine	Imine
MNC-316	600	93	97	3
MNC-317	700	67	55	12
MNC-318	800	43	34	9
MNC-319	900	32	13	19
MNC-356	600	85	80	19
MNC-357	700	70	82	18
MNC-358	800	43	74	24
MNC-359	900	20	69	28

[a] General reaction conditions: Benzyl alcohol, 1 mmol; Aniline, 1.5 mmol; KOH, 0.3 mmol; Temperature, 130°C; Time, 18 h; Catalyst, 20 wt% of benzyl alcohol; Atmosphere, argon.

[b] Substrate and product selectivity were determined by GC-FID using dodecanol as the external standard. The reactions were repeated two times and the average results are provided.

Table 7. Reactivity of different MNC catalysts for alcohol amination reaction as a function of different nitrogen species in the matrix.[a,b]

| Catalyst | N-content, % | | N3/(N1+N2) | Alcohol conversion, % | Product distribution, % | |
	N1+N2	N3			Amine	Imine
CSI-306[c]	--	--	--	7	5	3
CSI-306 (NH$_3$)	5.8	1.5	0.25	34	94	6
CSI-309[c]	0.6	0.5	0.8	12	72	28
CSI-309 (NH$_3$)	2.8	1.4	0.5	32	18	13
MNC-316	7.8	7.0	0.9	> 99	99	< 1
MNC-319	1.3	2.7	2.1	28	66	34
MNC-326	6.4	6.7	1.0	99	99	< 1
MNC-329	2.0	3.6	1.8	20	70	30
MNC-336	4.9	6.4	1.3	92	83	8
MNC-339	1.6	2.8	1.8	19	72	25
MNC-346	5.5	6.7	1.2	> 99	96	4
MNC-349	1.7	3.0	1.8	15	65	34
MNC-356	2.7 + 2.0	4.0 + 2.3	1.3[d]	85	80	19
MNC-359	1.1 + 1.8	2.1 + 3.5	1.9[d]	20	69	28

[a] General reaction conditions: Benzyl alcohol (1 *mmol*); Aniline (1.5 *mmol*); Catalyst (20 wt% of benzyl alcohol); KOH (0.3 *mmol*); Solvent, toluene (1 *mL*); Temperature (130°C); Time (18 *h*); Atmosphere (argon). [b] Substrate and product selectivity were determined by GC-FID using dodecanol as the external standard. The reactions were repeated two times and the average results are provided. [c] Carburized under argon atmosphere. [d] (N3+O2)/(N1+N2+O1).

Table 8. Deuterium labeling study; ^{1}H NMR and HRMS data.
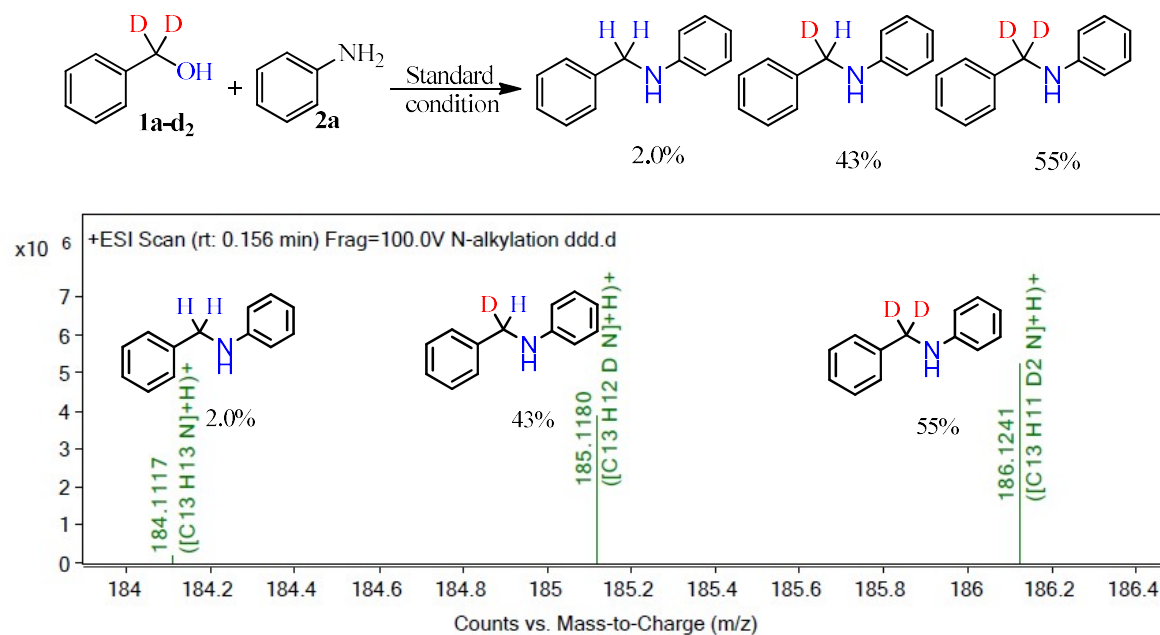
Property	3aa + 3aa-d$_1$	3aa	3aa-d$_1$	3aa-d$_2$
Signal, δ	6.67 [para-H (1H)]	4.20 [benzyl-H (2H)]	4.22 [benzyl-H (1H)]	---
Integral value	1.00	0.04/2.10 = 0.019	0.43	---
Calculated ratio	---	1.9 %	43.1 %	55 %
HRMS ratio	---	1.9 %	43.1 %	55 %

Table 9. Kinetic isotopic study ^{1}H NMR and HRMS data.
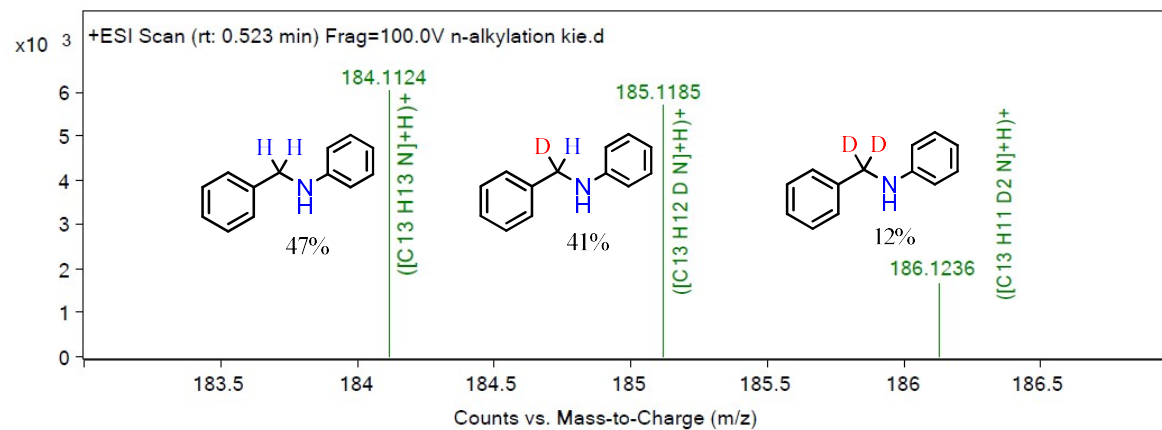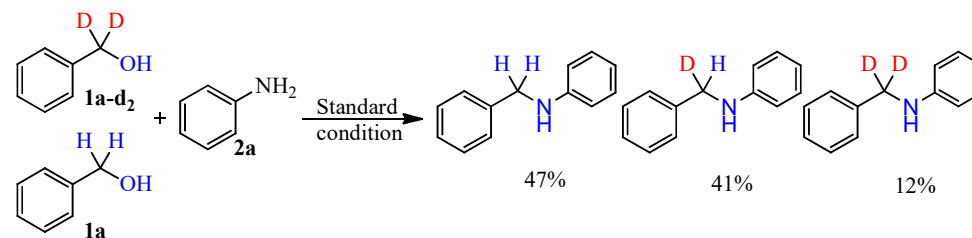
Property	3aa + 3aa-d₁	3aa	3aa-d₁	3aa-d₂
Signal, δ	6.68 [para-H (1H)]	4.21 [benzyl-H (2H)]	4.23 [benzyl-H (1H)]	---
Integral value	1.00	0.98/2.10=0.47	0.41	---
Calculated ratio	---	47 %	41 %	12 %
HRMS ratio	---	47 %	41 %	12 %
KIE		$K_{CHH}/K_{CDH} = 1.15$		

(a)

N3

N3

N1

N2

N1 – Phenanthridine-type

N2 – Acridine-type

N3 – Graphitic-type

(b)

N3

N4

N3 – Graphitic-type

N4 – Tris-s-triazine-type
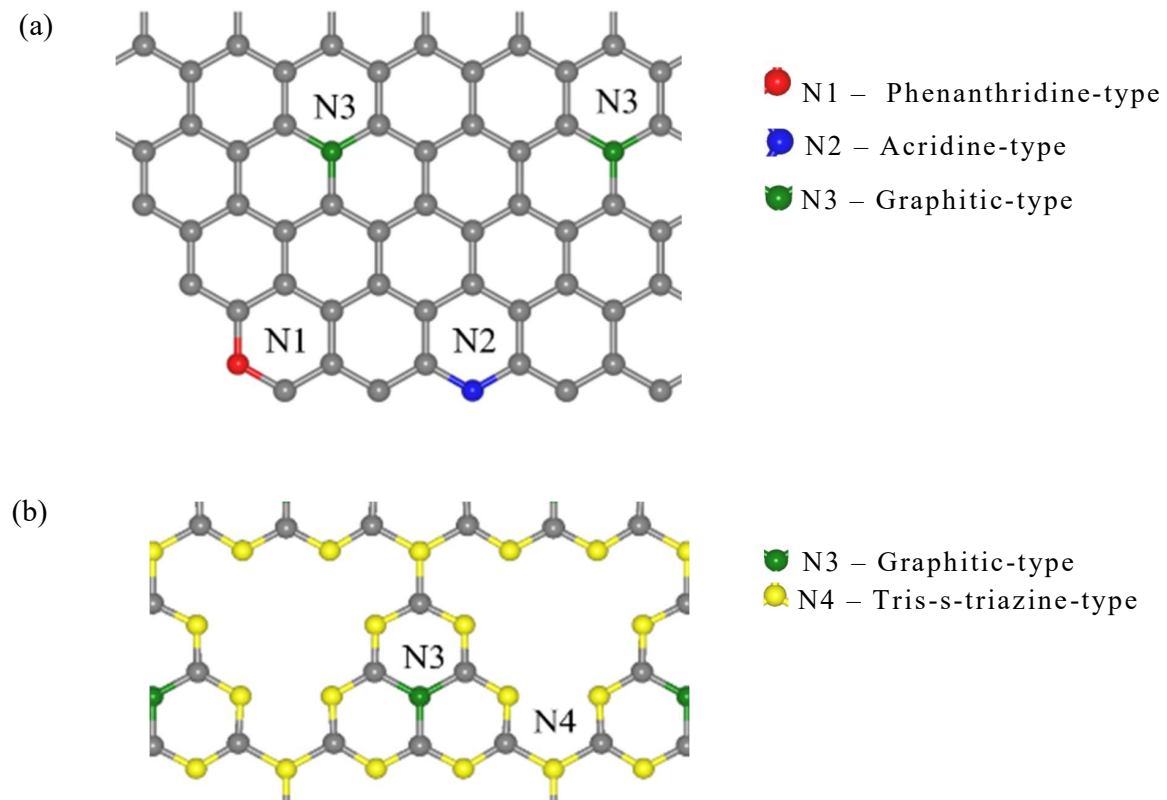
Figure 1. (a) The active *pyri*–N (N1 and N2) occurs as benzannulated pyridine, distributed at the edges/defects of the carbon matrix (MNC-*x*). (b) The inactive *pyri*–N (N4) occurs as *s*-triazine core (*g*-C_3N_4).
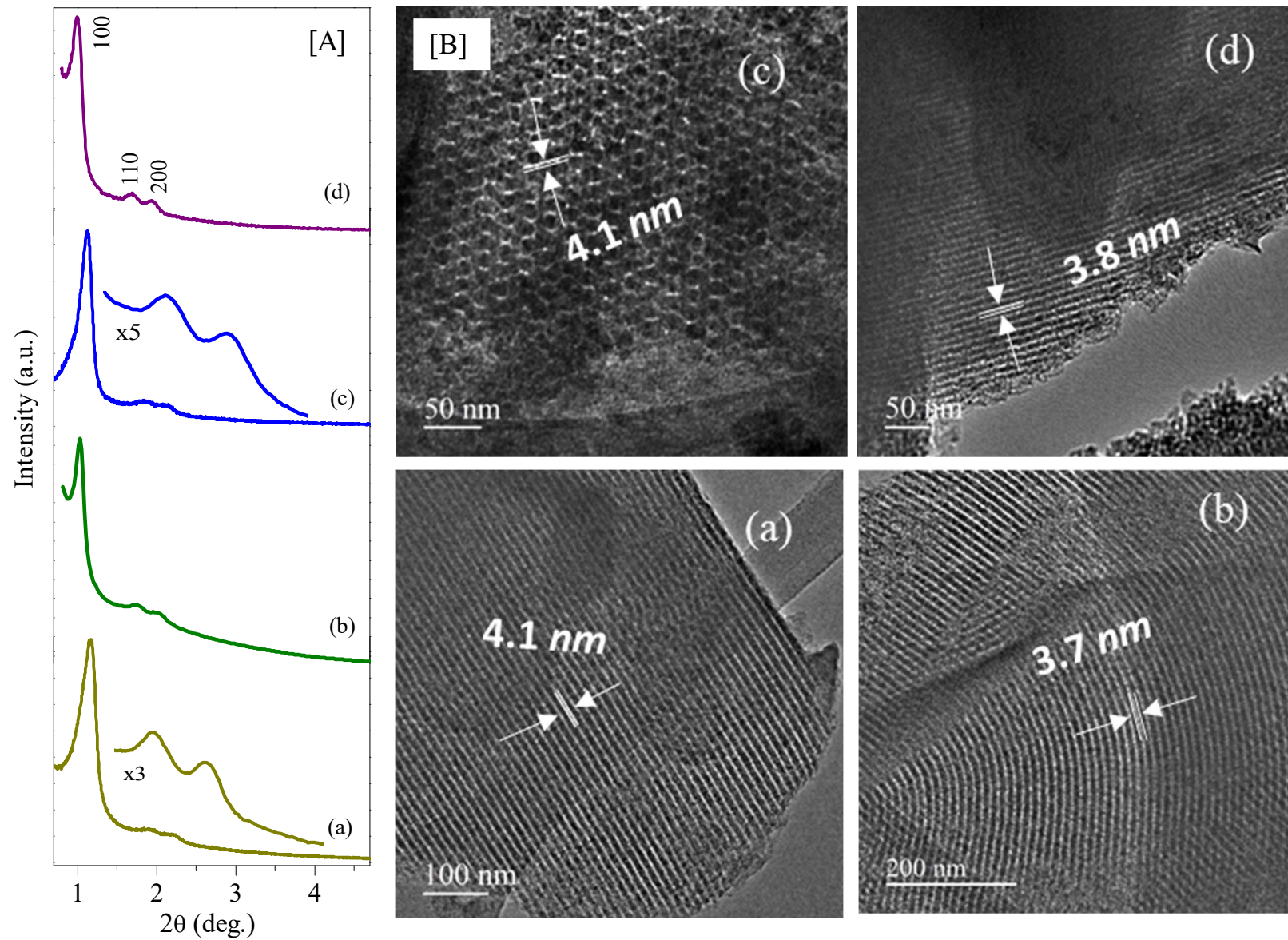
Figure 2. [A] Low-angle XRD patterns, and [B] HR-TEM images of: (a) CSI-306, (b) CMK-306, (c) MNC-316, (d) and MNC-326.
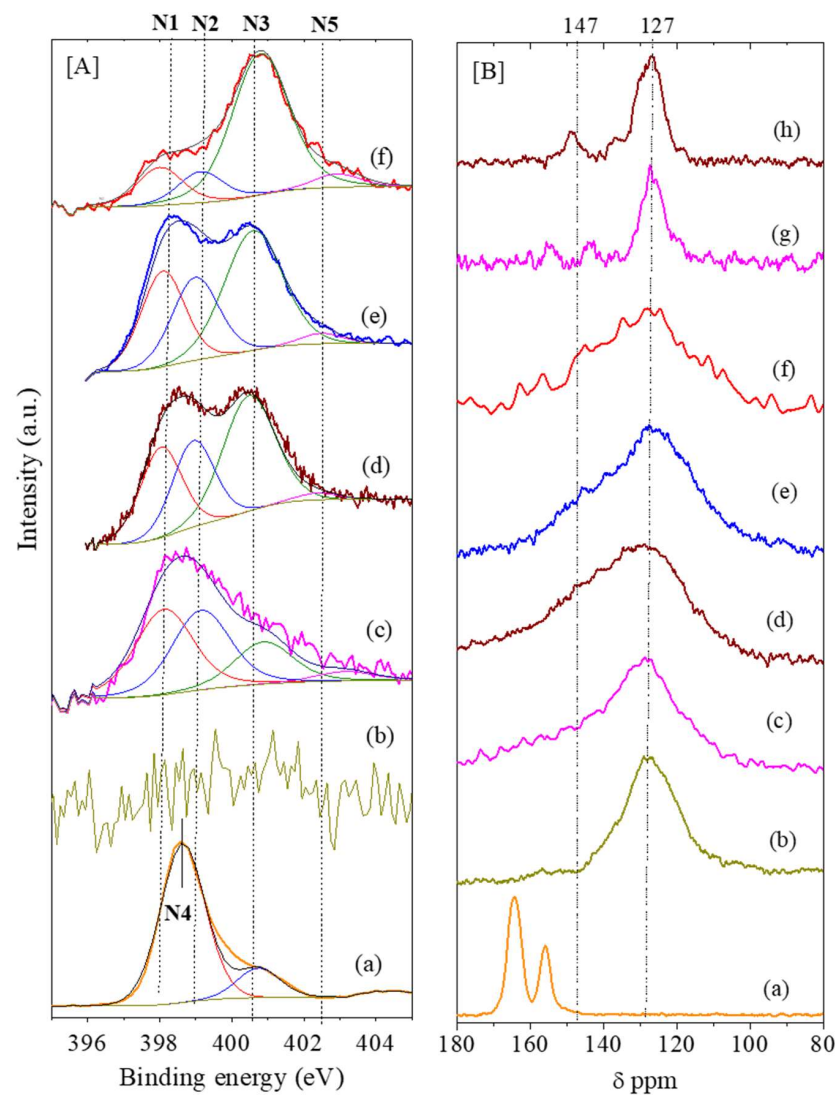
Figure 3. [A] N (1s) XP spectra of: (a) g-C$_3$N$_4$, (b) CSI-306, (c) CSI-306 (NH$_3$), (d) MNC-326, (e) MNC-316, and (f) MNC-319. The binding energy is corrected w.r.t. carbon, 284.5 eV. [B] ^{13}C MAS-NMR spectra of: (a) g-C$_3$N$_4$, (b) CSI-306, (c) CSI-306 (NH$_3$), (d) MNC-326, (e) MNC-316, (f) MNC-319, (g) phenanthridine and (h) acridine.

12
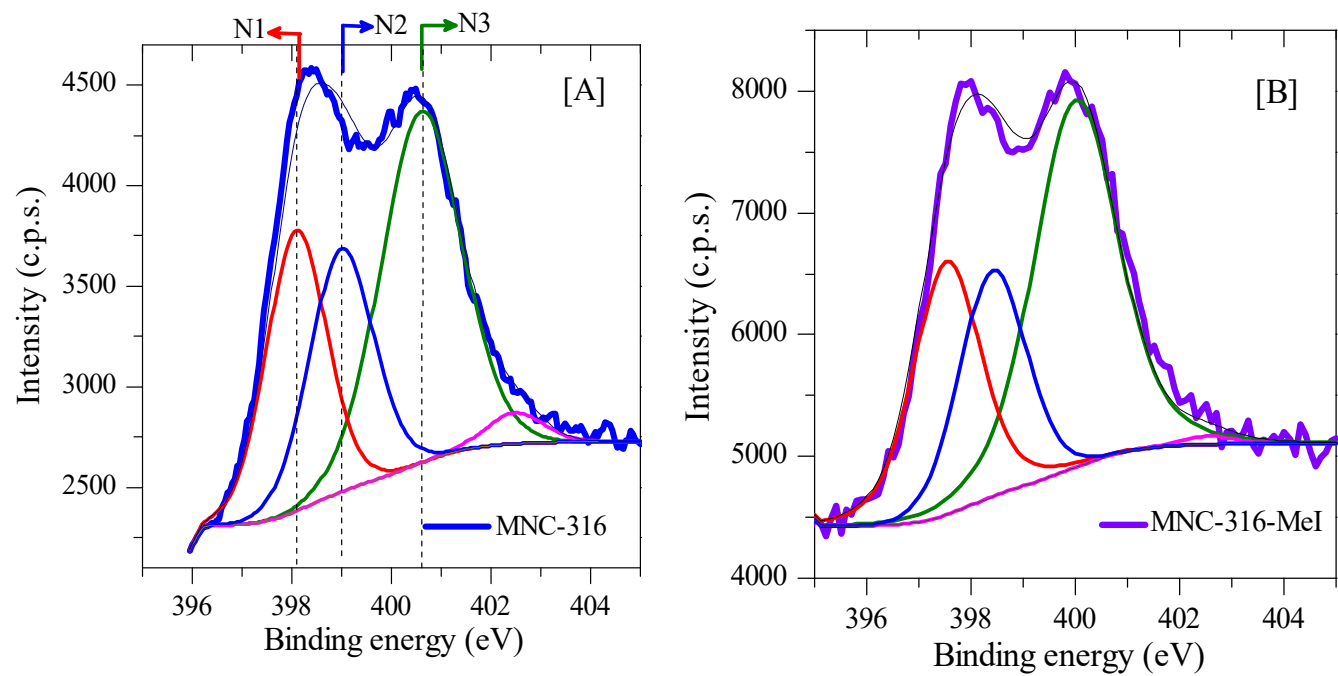
Figure 4. [A] N(1s) core level XP spectra of N−doped carbon showing phenanthridinic (N1), acridinic (N2) and graphitic (N3) nitrogen. [B] N(1s) core level XP spectrum of N-doped carbon treated with methyl iodide.
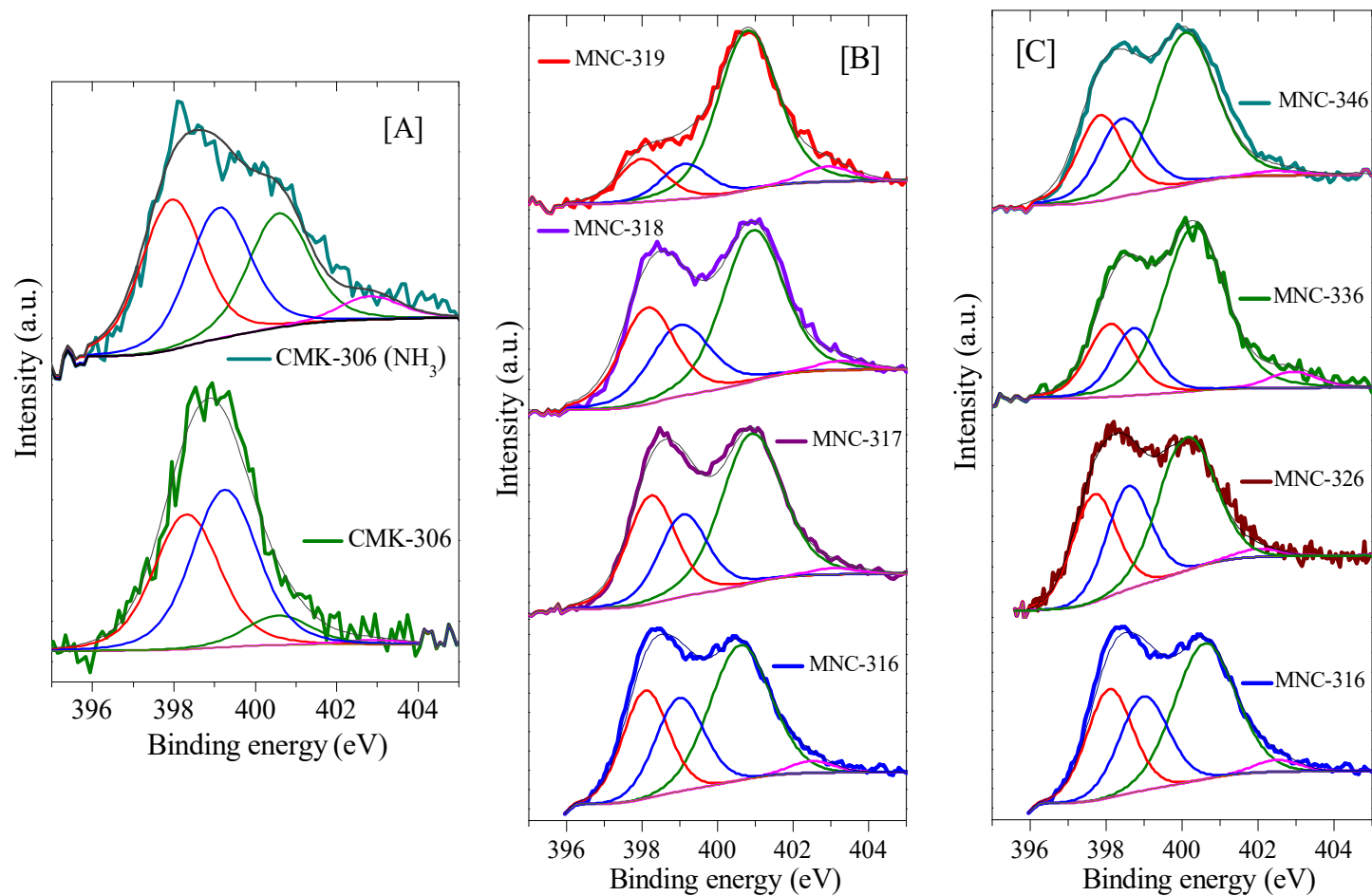
Figure 5. N(1s) core level XP spectra of various carbonaceous materials. [A] Sample pyrolyzed under nitrogen atmosphere and ammonia-treated at 600°C. [B] N-doped OMC pyrolyzed under nitrogen atmosphere in the temperature range 600-900°C. [C] N-doped mesoporous carbons prepared using different organic precursors, viz., ethylenediamine (MNC-316), *p*-diaminobenzene (MNC-326), aniline (MNC-336) and pyrrole (MNC-346).
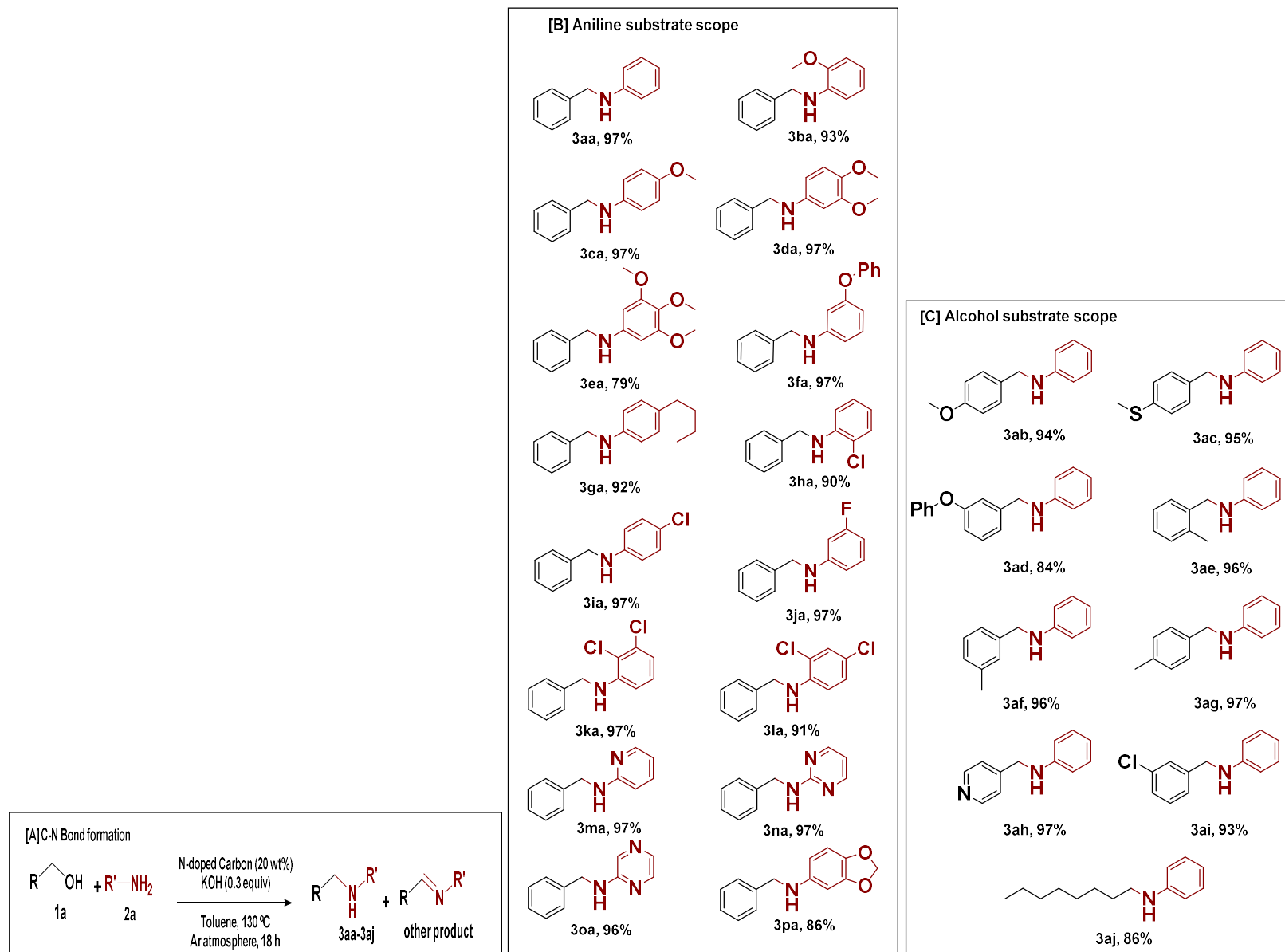
Figure 6. Synthesis of *N*-alkylamines and substrate scope: [A] Formation of *N*-alkylation of amines with alcohols. [B] Reactions of different amine derivatives with benzyl alcohol. [C] Reactions of different alcohol with aniline.
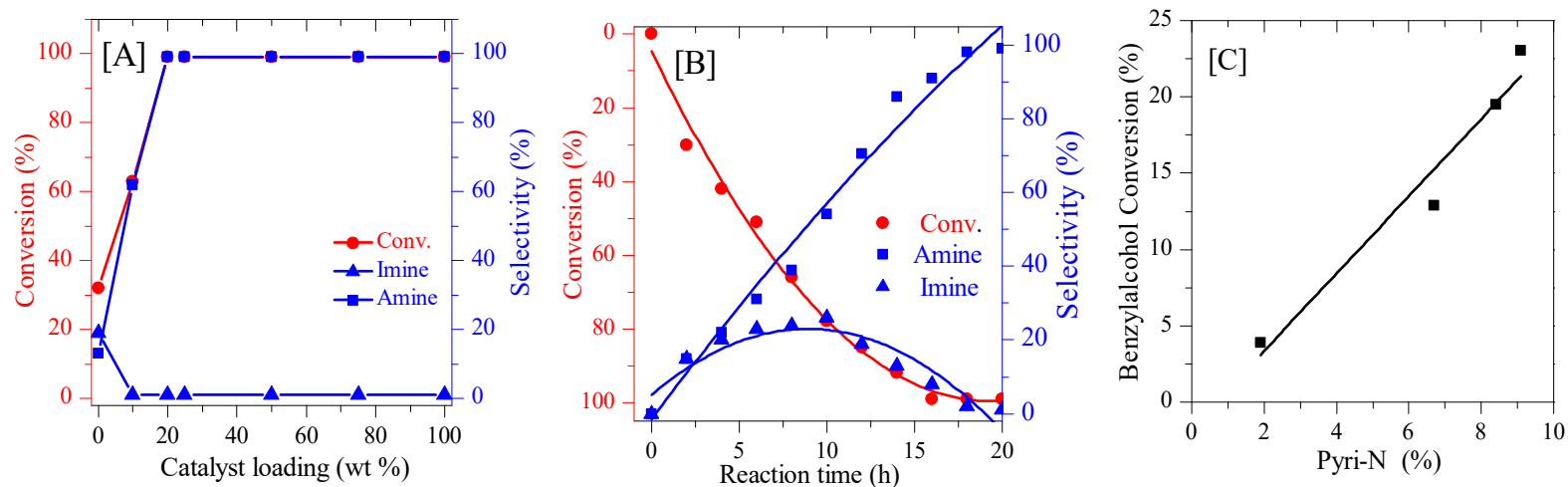
Figure 7. [A] Optimization of catalyst loading (Time, 18 h); [B] Effect of reaction time (kinetic plot) for the reaction of 1a with 3ac using MNC-316 catalyst; [C] A linear relationship between *pyri*-N content and benzyl alcohol conversion. <u>Reaction conditions</u>: Benzyl alcohol, 1 mmol; Aniline, 1.5 mmol; KOH, 0.3 mmol; Temperature, 130°C; Solvent (toluene), 1 mL; Reaction atmosphere, Ar. Substrate and product selectivity were determined by GC-FID using dodecanol as the external standard. The reactions were repeated two times and the average results are provided.
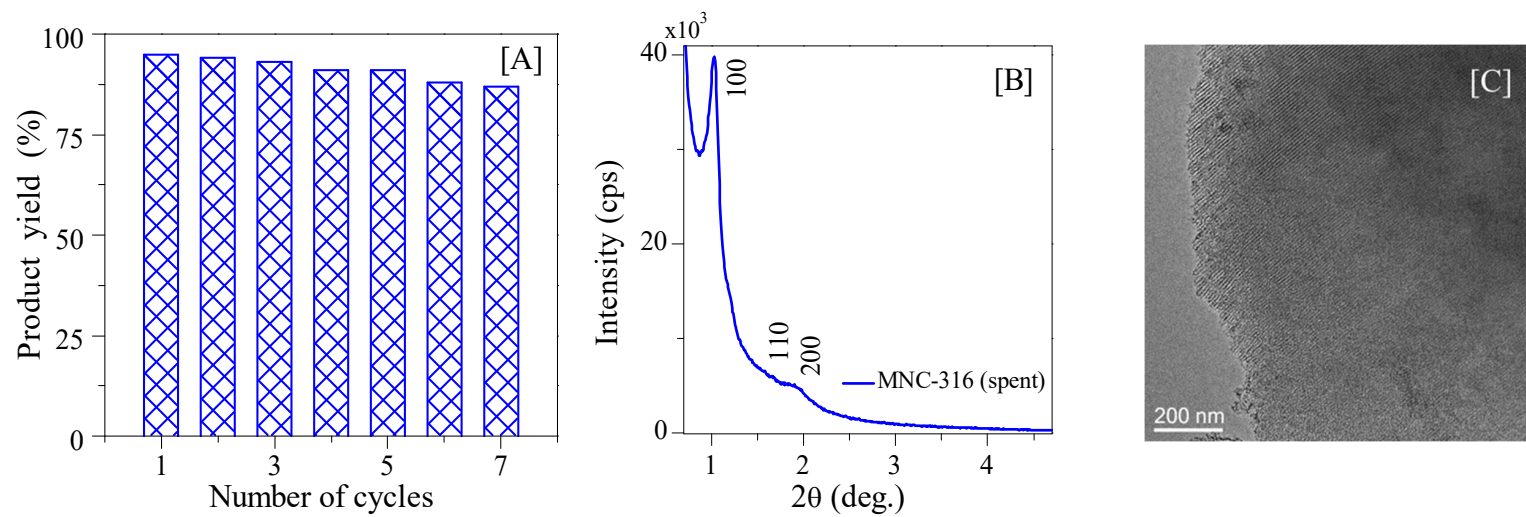
Figure 8. [A] Recyclability test of the catalyst (MNC-316) for seven successive runs; [B] XRD and [C] TEM image of spent catalyst (MNC-316) after seven successive cycles.
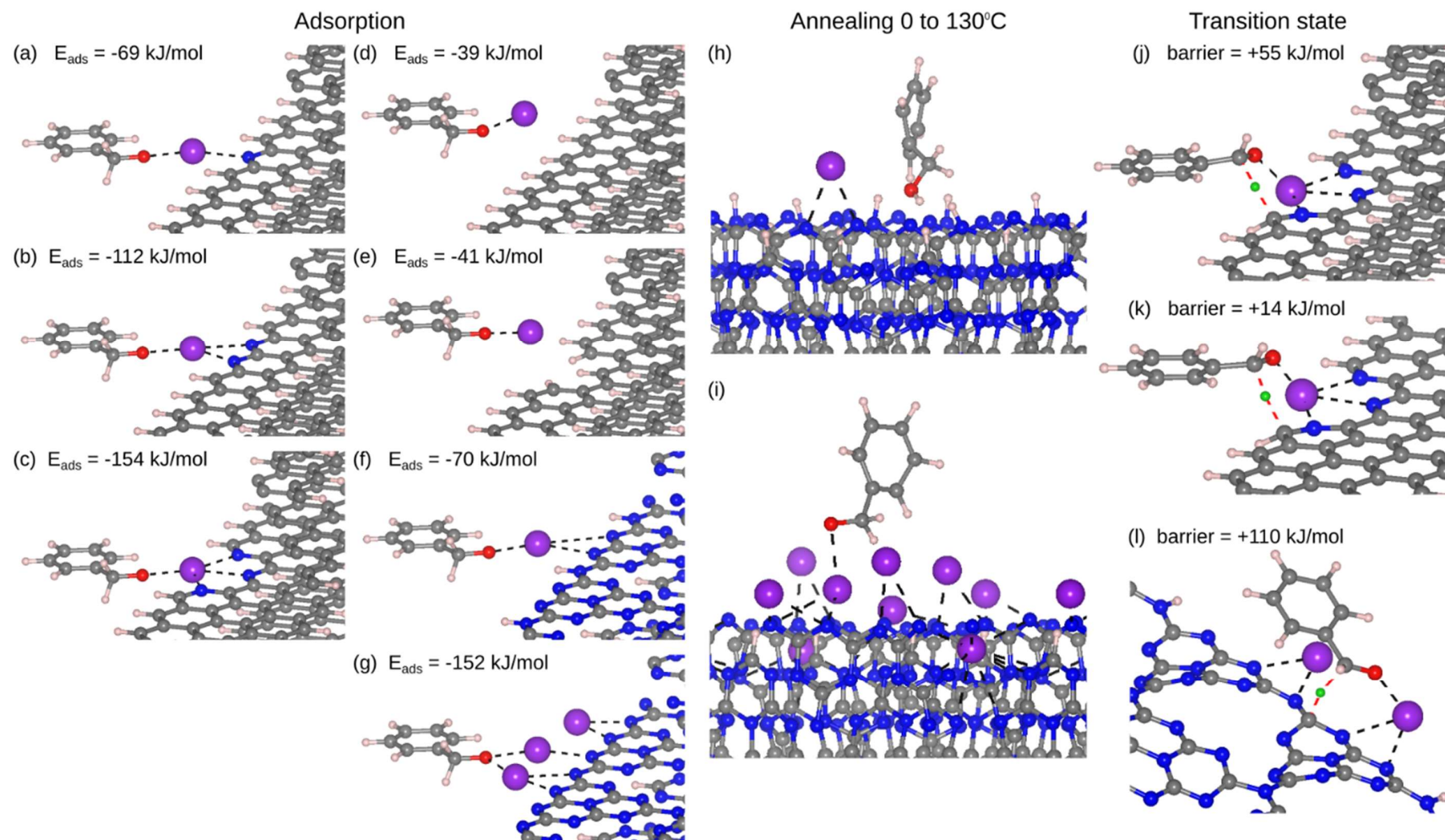
Figure 9. (a-g) Optimized structures for adsorption of potassium benzyloxide on: (a-c) N-doped carbon with an increasing number of N atoms; (d,e) carbon network with different edge cuts; (f,g) g-C_3N_4 with edge terminated with H or K atoms. Mesoporous carbon and g-C_3N_4 are represented by a truncated graphite structure with exposed edges terminated by H or K atoms, repeated periodically along the normal direction to the sheets; a vacuum layer is added along the parallel direction in order to represent the edges. (h,i) Snapshots after annealing optimized structure of potassium benzyl oxide adsorbed on (h) g-C_3N_4 with the edges terminated with H atoms, and (i) g-C_3N_4 with edges terminated with K atoms, 0-130°C, 2.5 ps. (j-l) Transition state for the transfer of a H⁻ ion from potassium benzyl oxide in three different models: (j) N-doped graphite; (k) a single sheet of N-doped graphene; (l) a single sheet of g-C_3N_4. In the case of (k) and (l), a vacuum gap of at least 15 Å is placed between periodic images along the normal direction to the sheets. Color code: H (white), H⁻ ion in the transition state (green), C (gray), N (blue), O (red) and K (purple).
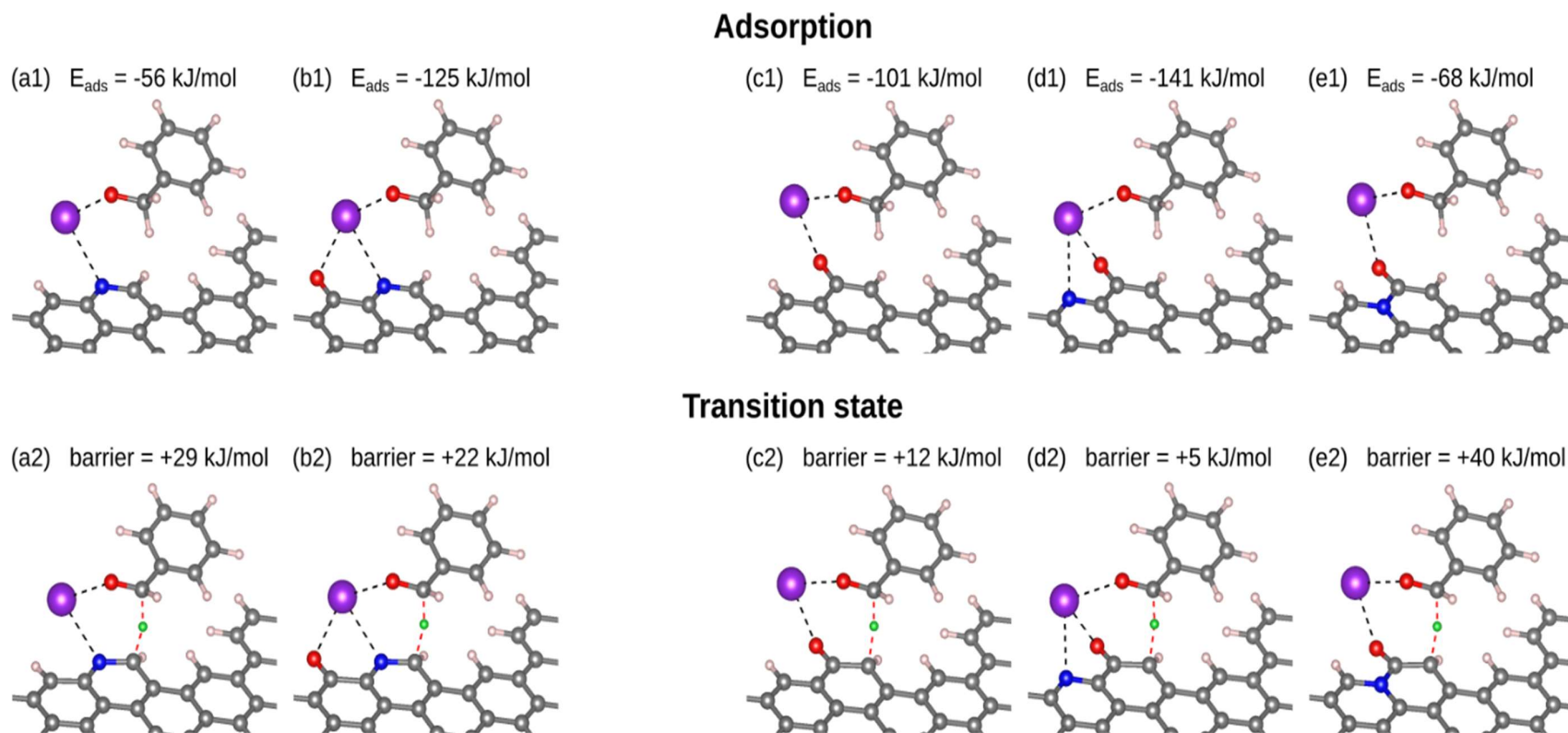
Figure 10. (Top row) Representation of the adsorption of potassium benzyloxide at the edge of graphene doped with nitrogen and oxygen (the adsorption energy E_{ads} for each system is provided as an inset). (Bottom row) Representation of the transition state for the transfer of the hydride ion from benzyloxide to a carbon atom at the edge of the graphene sheet (the barrier of the transition energy for each system is provided as an inset). (a) Adsorption at a pyridinic N. (b) Simultaneous adsorption at a pyridinic N and a carbonyl O, with the H^- transfer involving the graphene C directly binding the pyridinic N. (c) Adsorption at a carbonyl O. (d) Simultaneous adsorption at a pyridinic N and a carbonyl O, with the H^- transfer involving the graphene C directly binding the carbonyl group. (e) Adsorption at a carbonyl O, with a graphitic N directly binding the carbonyl group (amide group). Color code: H (white), H^- ion in the transition state (green), C (gray), N (blue), O (red) and K (purple).

19
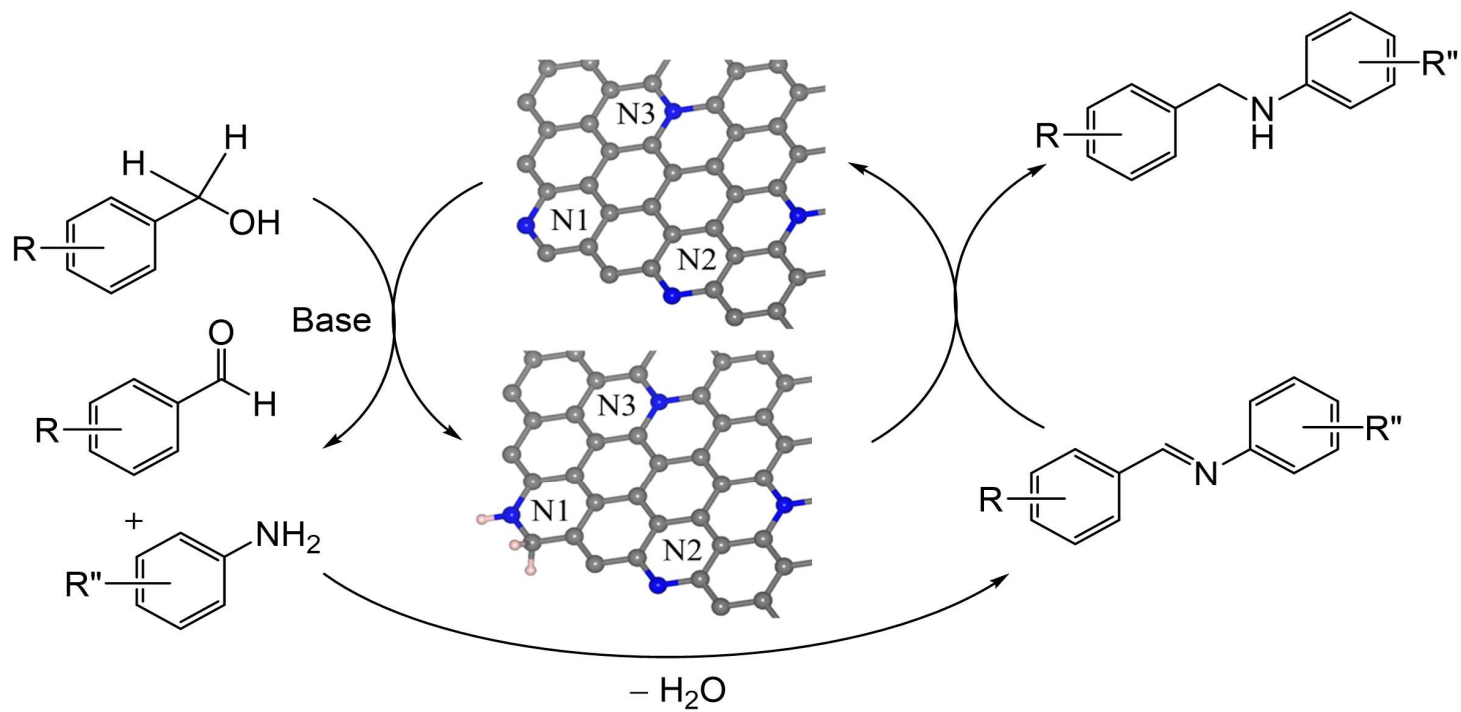
Figure 11. Mechanism for *N*-alkylation reactions on N-doped mesoporous carbon as heterogeneous catalyst.
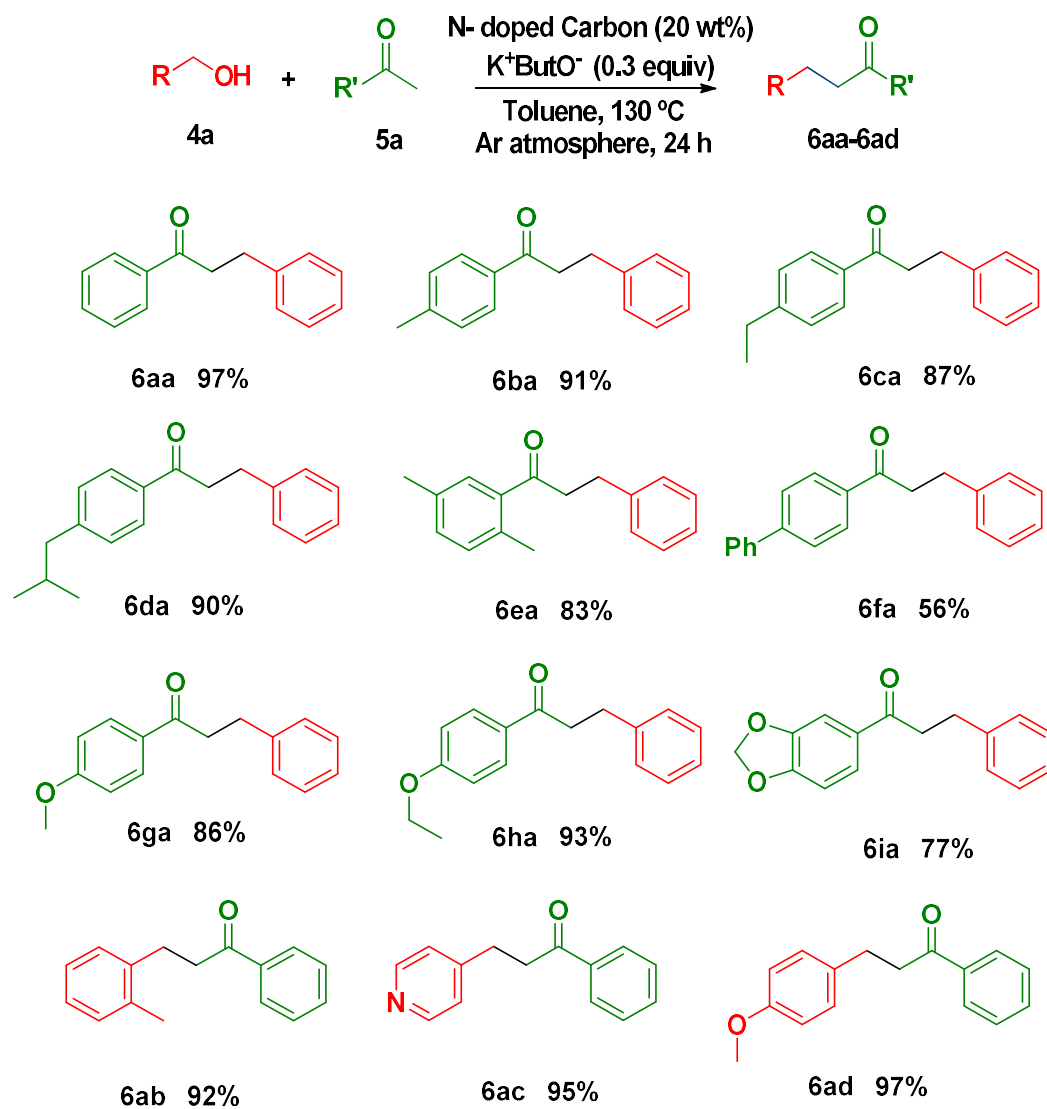
Figure 12. C-alkylation of α-methylketones with alcohols and substrate scope.
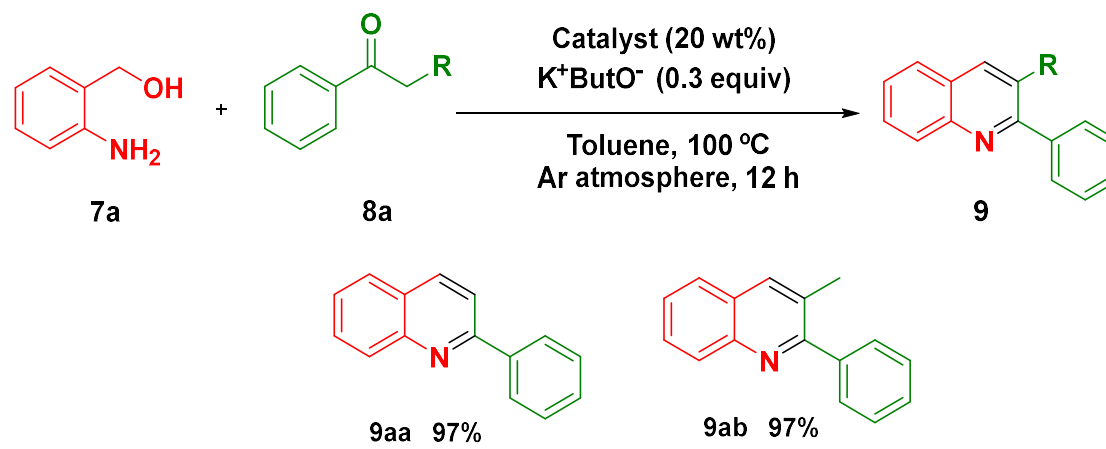
Figure 13. Synthesis of quinolines and substrate scope.